ABSTRACT

AUTO DETECTION IN AUTISM

by
Gayathri Chandar

Autism is a neurobiological disorder in which, certain regions of the brain are affected. The main features of autism are impairment in communication, social interaction, language and deficit in imitation and theory of mind. Using Functional Magnetic Resonance Imaging (fMRI), haemodynamic responses during a bilateral finger tapping task are analyzed for both autistic subjects and normal control subjects. fMRI is a noninvasive technique to image the activity of the brain related to a specific task. Generally, the active voxels in the fMRI images are detected using parametric or non-parametric statistical methods in which the fMRI response is assumed to have a model. Such methods are not applicable to detect the active voxels when the fMRI response is unknown. The data driven methods are also used for analyzing the fMRI data. The data driven methods are computationally expensive.

In this study, a method for detecting activated voxels without using prior knowledge of the input stimulus is presented. The assumption in this method is that the activation typically involves larger region comprising of several voxels and that these neighboring activated voxels are also temporally correlated. To validate the accuracy of this method, Principal component Analysis and Independent Component Analysis are also performed. A significant overlap in the sensorimotor cortex is found between the various methods suggesting that the automatic detecting method presented does provide accurate detection and localization.

AUTO DETECTION IN AUTISM

by
Gayathri Chandar

A Thesis
Submitted to the Faculty of
New Jersey Institute of Technology
in Partial Fulfillment of the Requirements for the Degree of
Master of Science in Biomedical Engineering

Department of Biomedical Engineering

May 2006

APPROVAL PAGE

AUTO DETECTION IN AUTISM

Gayathri Chandar

Dr. Bharat B. Biswal, Thesis Co-Advisor — Date
Associate Professor of Department of Radiology, UMDNJ

Dr. Tara Alvarez, Thesis Co-Advisor — Date
Assistant Professor of Biomedical Engineering, NJIT

Dr. Ronald Rockland, Committee Member — Date
Associate Professor of Biomedical Engineering, NJIT
Associate Professor of Engineering Technology, NJIT

BIOGRAPHICAL SKETCH

Author: Gayathri Chandar

Degree: Master of Science

Date: May 2006

Undergraduate and Graduate Education:

- Master of Science in Biomedical Engineering,
  New Jersey Institute of Technology, Newark, NJ, 2006

- Bachelor of Science in Instrumentation and Control Engineering,
  University of Madras, Chennai, India, 2004

Major: Biomedical Engineering

This work is dedicated to my

Father, Varadhan Chandar

Mother, Kalyani Chandar

Sisters, Malini Chandar and

Harini Chandar

ACKNOWLEDGMENT

I would like to express my earnest gratitude to my research co-advisor, Dr. Bharat B. Biswal, for extending me an inspiring guidance throughout this research work. It is difficult for me to express how grateful I feel for his kind supervision and patient mentorship during the duration of this research work.

Secondly, I would like to thank my research co-advisor, Dr. Tara L. Alvarez, for her constant support, guidance and valuable suggestions throughout this research study.

My heartfelt thanks are also due to Dr. Ronald Rockland, for his kindness in agreeing to be the committee member and for his valuable inputs during the review of this research work.

I also acknowledge the kindness of the colleagues working in the Radiology Department, University of Medicine and Dentistry, New Jersey, for extending their co-operation to me during my work.

Finally, I must acknowledge here the love, affection and continuous support of my elder sister Ms. Malini Chandar for her unstinted care and guidance to me all along.

TABLE OF CONTENTS

TABLE OF CONTENTS
(Continued)

TABLE OF CONTENTS
(Continued)

Chapter **Page**

LIST OF FIGURES

LIST OF FIGURES
(Continued)

CHAPTER 1

INTRODUCTION

Autism is a neurobiological disorder that affects the functioning of the brain which begins in childhood and persists throughout the adulthood. Autism was considered as a rare condition in 1943 with a prevalence of around 2-4 per 10,000 children. Several studies shows that the number of children diagnosed with autism have increased in recent years. According to the data from the United States Department of Education, in 1999 the autism incident rate was 4.5 cases per 10,000. The US centers for disease control (CDC) estimated 40 cases per 10,000 in 2005. The disorder is four times prevalent in boys than in girls and autism is prevalent regardless of any racial, ethnic or social group. [1].

The symptoms vary and not all symptoms are present in all autistic children. Some common symptoms in autistic children are: (i) lack of eye contact (ii) difficulty in understanding other's action and feelings (iii) loneliness (iv) resists change in routine (v) insensitive to pain etc.

Some theories also suggest a genetic basis to the disorder. It is usually associated with intellectual impairment. The brain structures affected in autism are cerebellum, cerebral cortex, limbic system, corpus collasm, basal ganglia and brain stem. Autism is usually characterized by (i) qualitative impairment in social interaction, (ii) qualitative impairment in communication, (iii) restricted, repetitive and stereotypical patterns of behavior, (iv) deficits in imitation and theory of mind and (v) a significant delay in language and cognitive development. Autistic children also have deficits in attention since the cerebellum is affected.

Bartholomeusz et al. [2] analyzed the head circumference in autistic children during the first two years of life. He found that the head circumference was at 25th percentile at birth and by 6-14 months it increased to 84th percentile in autistic children. Conciatori et al. [3] found an association between Hoxa1 poly morphism and enlarged head circumference in autistic children. Friedman [4] hypothesized that brain overgrowth was due to increased level of N-Acetylaspartate and to test this hypothesis, he used magnetic resonance spectroscopy (MRS) to measure N-Acetylaspartate where he found that it was reduced in cerebral regions. Other MRS studies [5-7] also found reduced N-Acetylaspartate in cerebellar and limbic system and reduced or normal level of N-Acetylaspartate in frontal and temporal lobes.

Akshoomoff et al. [8] conducted an MRI study and he found that in younger autistic children there was an enlargement in cerebral white and grey matter which accounted for an increase in the head circumference and this was not found in older and adolescent subjects with autism. Courchesne et al. [9] in a structural MRI study reported abnormal growth in autistic children during early life. They found hyperplasia of cerebellar white matter, neocortical grey matter and the growth was reduced in the subsequent years. Another important finding in their study was that the cerebral vermis lobes were found to be reduced in autistic children at all ages. They hypothesized the abnormal growth was due to (i) genetic factors (ii) excess number of axons and glial cells and (iii) elevated level of brain growth factor. Hashimoto et al. [10] and Levitt et al. [11] reported cerebellar vermis hypoplasia in autistic children from infancy to adolescent. Koul et al. [12] found that myelin composition was altered in autistic children and he hypothesized that myelin alteration was due to enlargement in the white matter.

Bauman et al. [13] analyzed the forebrain, brain stem and cerebellum of nine cases of autistic children. They found the neurons in the amygdala and hippocampus regions to be closely packed and small compared to the control group. The purkinje cells in the cerebral cortex were also reduced in the autistic children compared to the control group. They also observed the neurons in the septum part were larger in young autistic children compared to older individuals. A similar pattern of change in cell size was noted in the brainstem.

Using MRI, Carper et al. [14] found grey and white matter hyperplasia in the frontal, parietal and temporal regions in autistic children. In subsequent years the volumes were significantly reduced and there was minimal difference between autistic subjects and matched controls. In their study, they also found there was no significant difference in the occipital lobe of autistic children compared to the control group. Casonova et al. [15] reported small and underdeveloped cortical minicolumns in frontal and temporal areas in autistic children. Abell et al. [16] in a structural imaging study reported reduced amygdala volume.

Waterhouse et al. [17] hypothesized that the major autistic behavior is due to dysfunction of four neural mechanisms which are mentioned below:

- When the cell density of the neurons in the hippocampus is larger than the average cell density, the sensory component in the hippocampal system tissue fails to integrate and as a result the person cannot link the ongoing event with past event and this condition is termed as Canalesthesia.

- When the cells in the amygdala are immature, it cannot assign significance to incoming social stimuli such as facial expressions or messages and as a consequence other people's actions and messages are not understood.

- The neuropeptides namely vasopressin, oxytocin and serotonin (which are responsible for emotional states and behaviors) is disrupted. When this is disrupted the social behavior is affected.

- In healthy subjects, the temporal and parietal lobe is involved in facilitating polysensory organization. The polysensory organization of temporal and parietal lobe is disorganized and as a consequence there is a delay in shifting the attention and also the time spent in selective attention increases.

Nelson et al. [18] found an increased level of neurotrophin and neuropeptides namely vasoactive intestinal polypeptide, brain derived neurotrophic factor (BDNF), neurotrophin 4 (NT-4) and calcitonin a gene related protein in autistic children. Morrison and Mason [19] found an inverse relationship between the number of purkinje cells and the levels of BDNF and NT-4. Akshoomoff [8] concluded that autistic children have reduced number of purkinje cells due to an increased level of BDNF and NT-4.

Rodier [20] found that alleles of HOXA1 genes which is present in chromosome 7 was different in autistic children compared to a control group and this gene plays an important role in brain stem development. Since this gene is affected in autistic children, the author concluded that the lack of neurons in the brain stem is due to defect in HOXA1 gene.

Muller et al. [21] conducted an fMRI study to observe the functional organization during visually driven motor sequence learning. The activation in the superior parietal cortex was less pronounced in autistic group and the activation in prefrontal cortex and posterior parietal loci was greater in autistic children and the authors hypothesized that the axonal pathways connecting the cerebral deep nuclei, the thalamus and the cerebral cortex were affected in children with autism.

Allen et al. [22] conducted an fMRI study to determine the role of cerebellum in cognitive and motor functions. The activation was greater in cerebellum for motor tasks

compared to attention tasks in autistic children. The authors concluded that the reduced functional activation in the cerebellum for attentional tasks was due to a reduction of purkinje cells in the cerebellum. Baron-Cohen et al. [23] conducted an fMRI study to determine activation in the amygdala and the task was to identify the gender and mental state of the photographed person. The autism group demonstrated significant response in superior temporal sulcus compared to the control group and the control group demonstrated significant response in left amygdala, right insula and inferior frontal gyrus. The authors concluded the autistic children did not perform the task using amygdala and this shows that amygdala is affected in children with autism.

Hadjikhani et al. [24] conducted an fMRI study to examine the visual cortex and they reported the retinotopic maps in autistic children were similar compared to the control group. They concluded that low level visual processing is intact in children with autism.

Luna et al. [25] conducted an fMRI study in autistic children and subjects were asked to perform an oculomotor task and making saccades via a visual stimulus. During the oculomotor delayed response (ODR) task, there was no activation in the dorsolateral prefrontal cortex (DLPFC) and posterior cingulate cortex in autistic children. But there was activation in post parietal cortex, cortical eye fields, Medial Temporal (MT)/V5, temporal regions, anterior cingulate cortex, superior temporal sulcus, inferior frontal gyrus, insula, basal ganglia and thalamus and these regions are also involved in spatial working memory. It is established that the DLPFC plays an important role in spatial cognitive process. Since there was no activation in posterior cingulate cortex, they

suggested a functional disconnectivity exists in the frontal cortex and because of this disconnectivity autistics have deficits in higher order cognitive process.

Bailey et al. [26] in a postmortem study reported an increase in brain size and there were developmental abnormalities in the cerebral cortex, brain stem and cerebellum. Bauman et al. [27] and Rapin et al. [28] performed autopsy studies in autistic children and they found the cell density in amygdala was reduced.

1.1 Objective

The goal of this study is to use signal processing methodologies including motion correction, physiological noise reduction, and signal detection to improve reliable determination of task-related signal changes.

1.2 Overview

Functional Magnetic Resonance Imaging (fMRI) is an important and popular tool for studying the brain activity. The most frequently used effect to asses brain function is the blood oxygenation level dependent (BOLD) effect. High oxygenation levels represent high activity of brain regions responsible for performance of a specific task. The goal of fMRI data analysis is to detect the parts of the brain that are involved for a specific task. The data is usually preprocessed so that the artifacts due to motion and other sources contaminating the signal can be minimized. The functional activation maps can be generated using different techniques. In this study, three techniques were used and they are discussed briefly in this section and the remaining techniques are described in detail in Chapter 3.

A technique for thresholding was first introduced by Bandettini et al. [29], in which the shape of the response in a voxel is compared with the shape of the reference waveform. This technique is known as the correlation technique and is commonly used for analyzing the fMRI data. The correlation coefficient (cc) is calculated for each voxel. The advantage of the thresholding technique is that the noise is suppressed and in addition to it, the spurious correlation in voxels with very large signal changes arising from pulsatile blood flow and cerebro spinal fluid (CSF) flow is eliminated. The value of cc varies between + 1 to – 1 and the threshold value is varied between 0 and + 1. When the correlation coefficient is less than the threshold value, the data in each voxel is rejected.

The functional patterns in the functional imaging data can be isolated using Principal Component Analysis (PCA) and it was first introduced by Moeller et al. [30]. This technique measures the tendency of signals at all possible pairs of voxels to covary and the eigen vectors having the greatest variance in the data is determined.

McKeown et al. [31] used Independent Component Analysis (ICA) algorithm for analyzing fMRI data. In this method, the fMRI datasets are decomposed into spatially independent components. Each component consists of voxel values and time course of activation. The advantage of ICA is that it can differentiate task-related and nontask-related signal.

Levin et al. [32] proposed a new method for detecting brain activation in fMRI data and it s termed as Biasless Identification of Activated Sites by Linear Evaluation of Signal Similarity (BIASLESS). The analysis is based on the assumption that there is no change in the time course of signal in activated voxels when an entire task is repeated by

the same individual. The BIASLESS maps are generated by correlating the detrended time courses of the identified voxels during the consecutive scans of the same subject and the correlation coefficient is calculated for the two time series in each voxel of the brain. The activation of each voxel is detected in a manner that is independent of the presence or absence of activity in other voxels. Hence, this method does not require prior knowledge of the time course of the mental activity.

In this study, the task activated regions were identified automatically and the assumption is that the activation typically involves larger region comprising of several voxels and that these neighboring activated voxels are temporally correlated. Without prior knowledge of the reference waveform the activation maps were generated.

CHAPTER 2

MAGNETIC RESONANCE IMAGING (MRI)

2.1 Introduction

Nuclear Magnetic Resonance (NMR) was discovered in 1946 by Felix Bloch and Edward Purcell. When nuclei of certain atoms are placed in a magnetic field, they absorb energy in the radiofrequency range of the electromagnetic spectrum and this energy is reemitted when the nuclei are transferred to the original state and this phenomenon is termed as NMR. Magnetic Resonance Imaging (MRI) is a technique that uses NMR principles to acquire 2D and 3D images and it was illustrated by Lauterbur in 1973.

2.2 Physics of MRI

MRI makes use of the radio frequency RF region of the electromagnetic spectra to provide an image. It is a non-invasive technique that uses the principles of NMR.NMR property is exhibited by atoms having odd number of protons or neutrons. An example is Hydrogen. Hydrogen has a single proton in its nucleus so it has a net spin and magnetic dipole moment is associated with spin.

In order to create an NMR signal, a sample is placed in an external magnetic field Bo and the coil is placed near the sample with its axis perpendicular to the magnetic field. This coil acts as a transmitter and receiver. During the transmit phase, current is applied to the coil since the coil is in the magnetic field and current is applied, it creates an oscillating magnetic field in the sample. This oscillating magnetic field is known as RF pulse and the oscillations are in the radio frequency range so the coil is known as an RF

coil. During the receive phase, a signal is detected in the coil by connecting the coil to a detector in the external circuit.

The oscillating current (referred to as the Free induction decay) detected in the RF coil is known as Nuclear Magnetic Resonance (NMR) signal and its frequency is equal to the frequency of the RF pulse. The frequency at which it occurs is the resonant frequency of particular nuclei because at its resonant frequency, a nucleus is able to absorb RF pulse and returns a small portion of that energy back

2.3 MRI Scanner

The three main components of the MRI scanner are (i) the magnet, (ii) the gradient coils and (iii) the radio frequency coils. The other components are the shimming coils to ensure the homogeneity of the static magnetic field and specialized computer systems to control the scanner. [33].

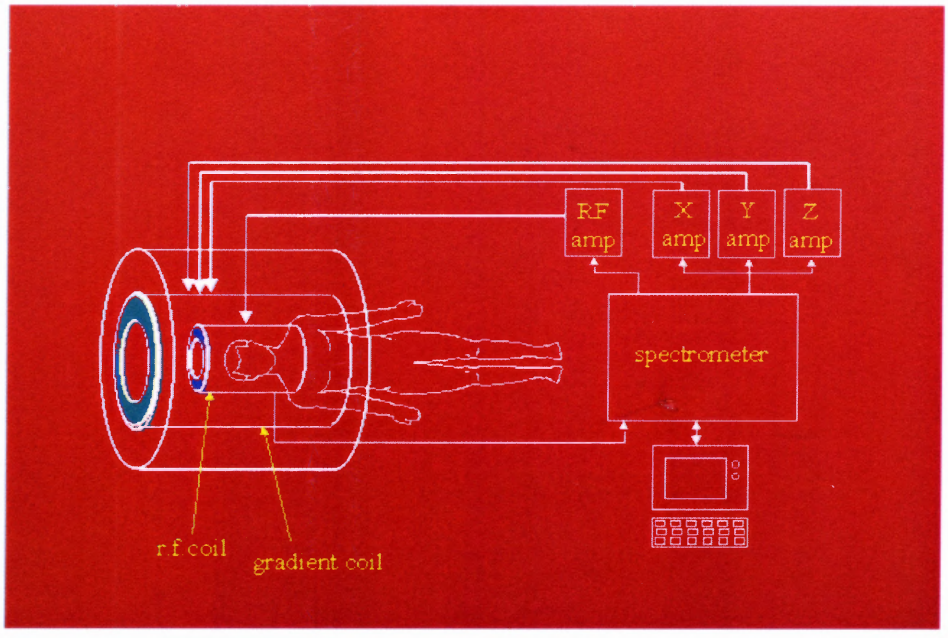

Figure 2.1 Block diagram of the MRI system.

2.3.1 Magnet

The static magnetic field is created by the magnet. The signal measured from a part of the body depends upon the strength and homogeneity of the magnetic field. In modern MRI scanners, the magnetic field is generated by the superconducting electromagnets. The field strength produced by the superconducting magnet is stable, homogeneous and the strength varies from 1 to 9 T for humans. Even higher field strengths are available for animal studies. A higher magnetic field is typically desirable for imaging because the signal strength generated by the number of precessing protons increases linearly with the magnetic field.

2.3.2 Gradient Coils

The gradient coil generates a linear magnetic field across the imaging plane. It is done to create a spatially dependent magnetic field such that each line in the space will have a different larmour frequency. The gradient coils generate a magnetic field that increases in strength along one spatial direction. The spatial locations are used relative to the main magnetic field with z going parallel to the main field and x and y going perpendicular to the main field.

2.3.3 Radiofrequency Coil

The RF coils transmit and receive the electromagnetic energy at the resonant frequency of the atomic nuclei. RF coils control the amount of energy that can be transmitted or received from the sample being measured. RF coils are placed between the object (for example head) to be imaged and the gradient coil to maximize signal. The MR signal depends on the sensitivity and uniformity of the RF coils.

2.4 Magnetic Field Gradients

In addition to the RF coils, there are three gradient coils in an MR scanner. Gradient is a linear position dependent magnetic field which is applied to alter the precessional frequency of the proton. The three gradient coils produce three gradient fields along X, Y and Z axis. The field produce by the gradient coil adds to the external magnetic field Bo and are much weaker in field strength. [34]. In order to extract the information about the spatial distribution of MR signal, three techniques are used namely which are described in the following sections:

2.4.1 Slice Selection Gradient, G_Z

Slice selection gradient (SSG) determines the slice that has to be imaged in the brain. For axial images, SSG is applied along the cranial-caudal axis. RF pulse is simultaneously applied with a certain frequency and the protons which has a precessional frequency equal to the frequency of RF pulse spins. Due to this gradient, proton excitation occur in a single plane and thus the signal is localized a dimension orthogonal to the gradient. It is the first of the three gradients applied to the sample volume.

2.4.2 Phase Encode Gradient, G_Y

Position of the spins in the third spatial dimension is determined by the G_Y gradient and is applied after the SSG. After the application of the SSG, all spins are in phase coherence. When this gradient is applied, the precessional frequency of the protons varies along the direction of the gradient. As a result, the protons precess at different rates and a phase difference is introduced. The phase shifts cannot be removed even after the gradient is turned off. Decoding the spatial position along the phase encoding direction occurs using a Fourier transform, only after all the data for the image have been collected.

2.4.3 Frequency Encode Gradient, G_X

The frequency encoding gradient is also called readout gradient and is applied in a direction perpendicular to SSG. For axial images, this gradient is applied across the X axis. When this gradient is turned on, higher precessional frequencies occur at the positive poles and lower precessional frequencies occur at the negative pole. The signal is amplified, digitized and is decoded by Fourier transform.

2.5 MR Signal Generation

When a proton is placed in an external magnetic field (Bo), the field exerts a torque on it that would tend to make it align with the field. Since the proton has a net spin, it posses an angular momentum thus it cannot align with the field so it precesses around the field axis and is shown in Figure 2.2. The frequency at which the protons precess is known as Larmor frequency and is proportional to external magnetic field Bo.

$$\nu = \gamma \, Bo \tag{2.1}$$

γ = Gyromagnetic ratio in MHz/T and is different for different nucleus.

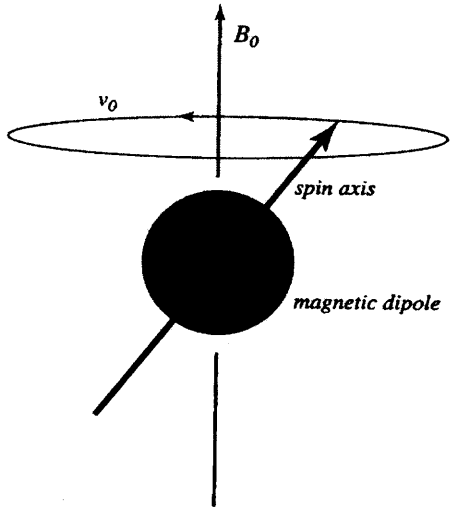

Figure 2.2 The magnetic field B_O exerts a torque on a nuclear magnetic dipole that would tend to make it align with B_O. Since the nucleus also has angular momentum, it precesses at an angle to the gravitational field. The precession frequency is proportional to the magnetic field and is the resonant frequency of NMR.

When the precession is observed for million of cycles, the dipole gradually aligns with the magnetic field Bo. Time constant for the relaxation is known as T_1. After several times longer than T_1, the dipole is aligned with Bo. The main magnetic field Bo is

generated by the scanner. In the absence of magnetic field, protons are not aligned and randomly oriented. However when placed in the magnetic field, part of it aligns with the magnetic field creating a net local magnetization M_O. M_O, which is the net difference between dipoles aligned with the field and opposite to the field, is proportional to proton density. It is weaker than Bo.

The net magnetization vector, M, is described by three components, M_Z is the component of the magnetic moment parallel to the applied field and is known as longitudinal magnetization. At equilibrium, the longitudinal magnetization is maximal and is denoted as M_O where $M_O = M_Z$, with the amplitude determined by the excess number of protons that are in the low energy state. M_{xy} is the component of the magnetic moment perpendicular to the applied magnetic field and is known as transverse magnetization. At equilibrium, the transverse magnetization is zero because the vector components of the spins are randomly oriented about 360 degrees in the x-y plane and cancels each other and is shown in Figure 2.3.

The oscillating magnetic field is generated by the RF coil. This oscillating magnetic field created in the sample is B_1 and is perpendicular to Bo and is less than Bo. The net magnetic field (vector sum of Bo and B_1) wobble around Bo. Initially, M_O is aligned with Bo but when net magnetic field is tipped slightly M_O precess around Bo. If B_1 is different from Larmor frequency, M_O wobbles slightly around Bo and if B_1 is equal to Larmor frequency, M_O tips farther away from Bo, tracing out a growing spiral as in Figure 2.4. When the RF pulse is turned off, M_O continues to precess about Bo. The effect of RF pulse is to tip M_O away from Bo and such pulses are described by the flip angle they produce. The flip angle depends on strength of B1 and duration of RF pulse.

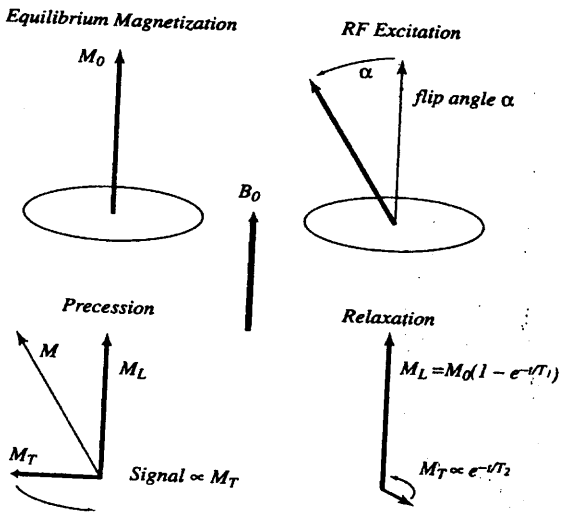

Figure 2.3 The net magnetization vector, M, is described by three components, M_Z is the component of the magnetic moment parallel to the applied field and is known as longitudinal magnetization. M_{xy} is the component of the magnetic moment perpendicular to the applied magnetic field and is known as transverse magnetization.

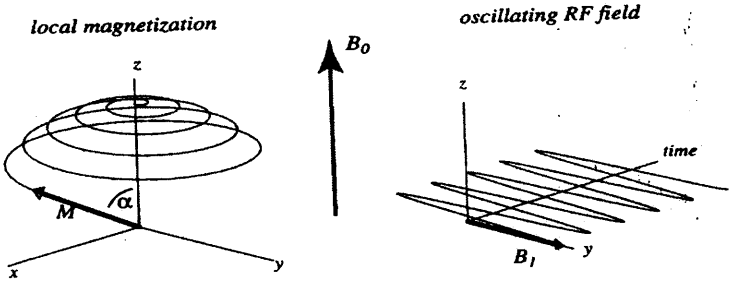

Figure 2.4 The RF pulse is a small oscillating field B_1 perpendicular to B_O that causes the net magnetic field to wobble slightly around the z-axis. As the magnetization M precesses around the net field, it traces out a widening spiral. M is tipped away from the longitudinal axis and the flip angle α is controlled by strength and duration of RF pulse.

A precessing magnetization creates a magnetic field and thus current is induced in the coil which creates an NMR signal proportional to the magnitude of the precessing

magnetization and the signal detected is called free induction decay. The name is derived because free refers to the free precession of the nuclei; induction is an electromagnetic process by which a changing magnetic field induces current in the coil and decay describes the signal is transient.

The signal decays exponentially in amplitude with a time constant T_2 as in Figure 2.5. The exponential relationship is given by,

$$M_{xy}(t) = M_O e^{-(t/T2)} \qquad (2.2)$$

When t=0, $M_{xy=} M_O$ and when t= T_2, M_{xy}=.37 M_O

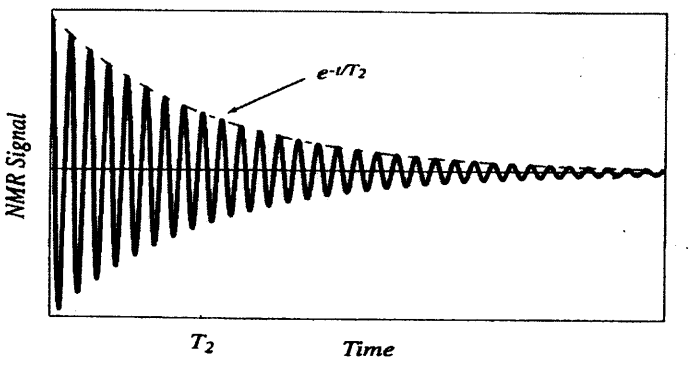

Figure 2.5 After a 90^0 pulse tips the longitudinal magnetization into transverse plane, a detector coil measures an oscillating signal which decays in amplitude with a time constant T_2.

The experiment is repeated to generate a new signal and the time between RF pulses is called the repetition time (TR). When TR is long, the signal generated by a second RF pulse is the same as that of the signal generated by the first RF pulse and when TR is short, the signal generated by second RF pulse is weak.

2.6 Contrasts in MRI

Unlike other imaging modalities, in MRI a number of different contrast mechanism are present which can be used simultaneously to maximize the contrast from the various mechanisms. The main contrast mechanism sources are due to longitudinal relaxation (T_1), transverse relaxation (T_2), and proton density. Two other sources of mechanism including diffusion and chemical shift also exists, but are not very often used for brain imaging. Contrast in an image is proportional to the difference in signal intensity between the adjacent voxels in an image. T_1 and T_2 are physical properties of the tissue and TR and TE are the pulse sequence controls on the MRI machine. When T_1 and T_2 between two adjacent voxels changes, the signal in those two voxels changes thus creates contrast with an MRI image. By changing the pulse sequence parameters TR and TE, the contrast dependence in the image can be weighted toward T_1 or T_2. [35].

2.6.1 T_1 Weighted Image

T_1 is the time constant that describes the recovery of the longitudinal component of net magnetization over time. Every tissue has its own T_1 and T_2 value. In T_1 weighted images, most of the contrast between tissues is due to difference in T_1 value. T_1 contrast is approached by imaging with a short TR and short TE, compared to tissue T_2 so that image contrast due to T_2 is reduced.

2.6.2 T_2 Weighted Image

T_2 is the time constant that describes the decay of the transverse component of net magnetization over time. Images created with TR's and TE's to enhance T_2 contrast are referred as T_2 images. The contrast of T_2 weighted image is dependent on T_2 and this T_2

dependence is increased by using a long echo time and long TR compared to T_1 so that image contrast due to T_1 is reduced.

2.6.3 Proton Density Weighted Image

In this type, the contrast is dependent on the density of protons in the tissues. Proton density weighted images are generated by choosing $TR > T_1$ and $TE < T_2$ When there are more number of protons in a given tissue, that specific tissue appears bright.

2.7 Pulse Sequences

A pulse sequence is a set of RF and gradient pulses to the sample to produce a specific form of NMR signal and is repeated several times during the scan. The characteristic of MR images depends on the amplitude and shape of the gradient and also the time interval between pulses.

MR relies on three major pulse sequences namely the spin echo, inversion echo and gradient recalled echo which are described in the following sections:

2.7.1 Spin Echo

It describes the excitation of the magnetized protons in a sample with an RF pulse and production of FID, followed by a second RF pulse to produce an echo. Due to 90^o RF pulse, transverse magnetization M_{xy} is maximum and the spins are in phase. After a delay of TE/2, 180^o RF pulse is applied and as a result the phase difference is introduced in the spins. The spins which are rephased produce a measurable signal equal at a time equal to the time of echo (*TE*). Echo reforms in the opposite direction from the initial transverse magnetization vector, so spins experience opposite external magnetic field

inhomogeneties and this strategy cancels their effect. The amplitude of the echo is determined by T_2.

2.7.2 Inversion Recovery

An initial 180° RF pulse inverts the longitudinal magnetization of tissues, M_Z to - M_Z. A 90° RF pulse rotates M_Z into the transverse plane to generate an FID. The time delay between 180° RF pulse and 90° RF pulse is known as time of inversion (TI) and it controls the contrast of the tissues. Inversion recovery sequence produces a negative longitudinal magnetization that results in negative or positive transverse magnetization and the signals are encoded.

2.7.3 Gradient Recalled Echo

A magnetic field gradient is induced for the formation of an echo instead of 180° RF pulse. The strength of the local magnetic field changes due to this magnetic field gradient. FID signal is generated under a linear gradient, the transverse magnetization dephases rapidly as the gradient is applied continuously. A gradient echo is produced, if the polarity of the gradient is changed and echo formation is due to rephrasing of the spins. The echo will decay if the gradient is applied continuously and the signal can be acquired. The tissue contrast is determined by flip angle.

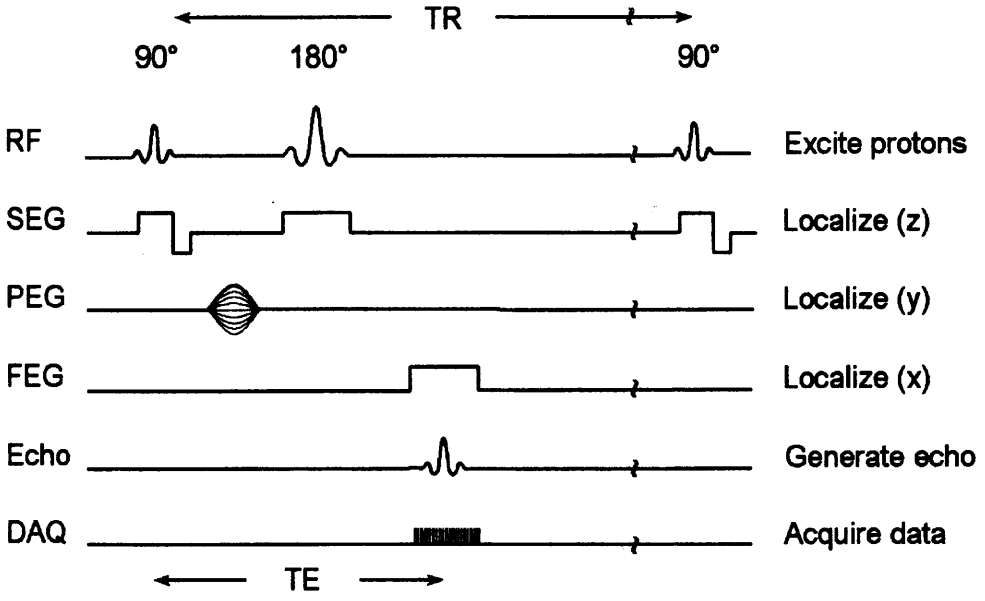

Figure 2.6 Spin echo pulse sequence timing diagram indicates the timing of SSG, PEG and FEG during the repetition time (TR), synchronized with the RF pulses and the data acquisition (DAQ) when the echo appears.

2.7.4 Echo Planar Imaging

EPI is an MR acquisition method that collects all the data required to fill all the lines of k space from a single echo train. In this technique, multiple echoes are generated and each is phase encoded by a different slope of gradient to fill all the required lines of k space. Echoes are generated either by 180 deg rephasing pulses termed spin echo EPI or by gradients termed gradient echo EPI. In order to fill the entire k space in one repetition, the readout and phase encode gradients must rapidly switch on and off.

In conventional spin echo, one line of k space is filled for every TR. The position of this line depends on the amplitude and polarity of the phase gradient. The amplitude and polarity of the read out gradient does not change and each line is filled in the same direction. Using EPI, the entire k space is filled after the application of single excitation

pulse. In EPI, the read out gradient is rapidly switched from positive to negative; positively to fill the k space from left to right and negatively to fill the line from right to left. The polarity of the phase gradient does not have to be changed. The first application of the phase gradient is positive to fill the top line. The next application to encode the next echo is still positive but its amplitude is slightly less thus the next line down is filled. This process is repeated until the centre of k space is reached where the polarity of the phase gradient becomes negative to fill the bottom lines. [36].

Summary

This chapter discussed the basic physics of Magnetic Resonance Imaging (MRI) and also about the generation of MR signal. To create an NMR signal, an external magnetic field, gradient coil and radiofrequency coil are needed. The external magnetic field is always generated by the scanner. The radiofrequency coil transmits and receives the electromagnetic energy and the gradient coil generates a linear magnetic field to alter the precessional frequency of the proton. The contrast in the image depends on the tissue properties namely T_1, T_2 and proton density. The functional MR images are obtained with the help of echo planar imaging pulse sequence.

CHAPTER 3

FUNCTIONAL MAGNETIC RESONANCE IMAGING

Signal intensity of MR images can be altered when there is a change in blood oxygenation and this phenomenon was first observed by Ogawa. With this phenomenon, one can observe both the anatomical structures of the brain and also the function of structures participated for a specific task. This type of imaging is known as Functional Magnetic Resonance Imaging (fMRI). Fully oxygenated blood has the same susceptibility as other tissues in the brain but deoxygenated blood changes the susceptibility since it is paramagnetic. When the blood is deoxygenated, field distortions around the vessel is increased so there is a drop in the MR signal. If the blood is oxygenated, the intensity of the signal increases. When neural activity is increased in a region of the brain, there is an increase in neuronal firing that leads to more metabolic consumption. Decrease in the oxygenation leads to vasodilation resulting in increased blood flow in the active regions. However, the increase in oxygenated red blood is much more than the metabolic need at the active regions. As a consequence, there is an excess of oxygenated red blood cells in the active regions. Because, oxyhemoglobin and deoxyhemoglobin red blood cells have different magnetic properties, an increase in the ratio of oxyhemoglobin to deoxyhemoglobin red blood cells causes less spin dephasing and causes the MRI signal intensity from the activated regions to increase. This BOLD contrast is the basis of most of the fMRI studies.

BOLD effect is the result of two factors:

- Deoxyhemoglobin produces a magnetic field around the blood vessel and as a result an MR signal is reduced.

• Brain activation is characterized by a drop in Oxygen Extraction Fraction (OEF) which results in a drop in oxyhemoglobin thus the MR signal is increased.

The prototype brain mapping experiment consists of alternating periods of stimulus task and control task and the cycle is repeated several times. Images are collected throughout the cycles and the image acquisition is repeated at several intervals of the time of repetition (TR) throughout the experiment, while the subject alternates between the stimulus and control task. In every experiment it is assumed that the magnitude of the BOLD effect reflects the magnitude of the neural activity change [34].

3.1 Paradigm Design

A standard method of task presentation uses a box-car or block design where blocks of the stimulus or task are presented typically for 20-30 seconds, alternating with periods of rest or a control condition. Throughout these stimulus/control cycles dynamic echo planar images are collected covering all or part of the brain. In order to accommodate the haemodynamic response, the duration of the task should be long in the order of minutes. The control task is chosen carefully such that it activates all of the neural processes common to the stimulus-task. By subtracting the brain regions recruited during the performance of the control task from the brain regions recruited during the test condition, the areas of the brain whose activity is associated specifically with the cognitive process of interest can be identified.

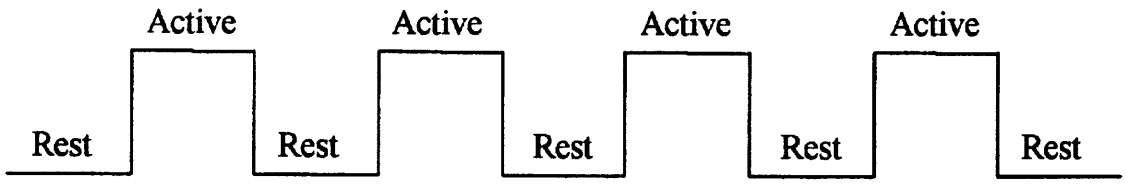

Figure 3.1 Representation of box car waveform.

An alternative experimental approach is to present stimuli as isolated brief events separated in time so that the individual response to single events can be identified. The principle advantage of this event-related approach is that, it avoids the potential confounding factors of habituation or fatigue which may arise in a block design as a consequence of the presentation of repeated identical stimuli.

3.2 Analysis of fMRI Data

fMRI data from a single run consists of a time series of 3D images while the subject is inside the scanner. The main objective in the experiment is to find the regions of the brain that is activated for a given task and the activation maps can be generated by correlating the time series with the given task. The pre-processing steps that are usually performed on the raw data are image registration and smoothing. Registration is usually done to correct for subject head movement during the experiment and smoothing is done to increase the signal to noise ratio.

3.3 Motion Correction

Any motion during the acquisition of an MR image will produce artifact and such motion include subject head movement, coughing, swallowing, and physiological motions such as blood flow, respiratory motions and CSF motions. Even with a slight head movement (~1mm) by the subjects during image acquisition motion artifacts are produced. This is a major problem because different samples in k space are inconsistent with one another [31] and the interpretation becomes problem. This makes analyzing data difficult and image registration is routinely used to minimize the effects due to motion induced signal changes. Registration is usually done to eliminate the artifact due to motion. Registration is a technique in which two or more images are aligned so that they superimpose perfectly. It is usually done by transforming an input image and comparing it with a base image. The transformation is repeated until the input image resembles the base image. The two main algorithms used for registering MR images are described below:

3.3.1 Least Square Measure

MR images can be registered using a least square similarity method which was proposed by Hajnal et al. [37] The least square similarity is given by

$$LS(u,v) = \sum_{i=1,j=1}^{i=n,j=m} \left(u(i,j) - v(i,j)\right)^2 \Big/ N \qquad (3.1)$$

where u and v are the given two images, i and j varies from 1 to n and 1 to m respectively, n and m represents the number of voxels in the x and y dimension of the images u and v respectively, N is the number of voxels in the overlapping region of the

two images and $u_{(i,j)}$ and $v_{(i,j)}$ represent signal intensity at voxel site (i,j) of the images u and v respectively.

This method cannot be used to register the images obtained from different modality because the tissue has different intensity values for different modalities. T_1 and T_2 weighted images cannot be registered using this method.

3.3.2 Automated Image Registration (AIR) Method

Woods developed an automated registration algorithm for PET images and have since extended this method for MRI. This method is based on the assumption that for two given images, the value of any voxel in one is directly proportional to the value of the corresponding voxels in other images only if the images are perfectly aligned. If they are misaligned the values change from voxel to voxel throughout the image. Based on the intensity value of the voxels, the brain is first segmented using a threshold.

If u is the reference image and v is the test image then the ratio r is given by r(i) = u(i) / v(i) where u(i) is the value of voxel i in image u and v(i) is the value of the corresponding voxel in image v. The normalized standard deviation is given by r_{std} / r_{mean} where r_{std} is the standard deviation of r and r_{mean} is the mean value of r over all voxels. The test and reference images are interchanged and now u is the test image and v is the reference image and the new normalized standard deviation of r is calculated and is given by r'_{std} / r'_{mean}. The ratio R_{std} / R_{mean} is generated where $R_{std} = (r_{std} + r'_{std}) /2$ and $R_{mean} = (r_{mean} + r'_{mean})/ 2$. The main aim of the algorithm is to minimize the ratio of R_{std} / R_{mean} so that the voxel to voxel variation is minimized [38].

3.4 Statistical Analysis of fMRI Data

The fMRI data provides a time series of images (samples) for the volume scanned in a sequential fashion. This allows time-series analysis for every voxel in the brain for the entire volume. Several methods have been proposed to detect and identify activated voxels in the brain and generate task–dependent activation maps. In order to yield rigorous maps and quantify the task-induced signal changes, a number of approaches can be applied. Analysis methods are required to find the response waveforms and associated activated regions. These methods can be divided into two categories depending on whether or not they require prior knowledge about activation patterns: model-based and model-free [39]. Although the model based methods are easy to implement and are effective in analyzing data with simple paradigms, they are not applicable in situations in which pattern of neural response are complicated and when fMRI response is unknown. The two model free methods used for the analysis of fMRI time series are Principal Component Analysis (PCA) and Independent Component Analysis (ICA).The following section describes both the model free and model based techniques used for analyzing fMRI data.

3.4.1 Parametric Methods

In parametric method, the data is assumed to follow a common distribution like normal distribution and the statistics are calculated based on that assumption. The statistical tests based on the parametric statistics are called parametric statistical tests. The following section explains some of the commonly used statistical tests.

3.4.1.1 Subtraction Technique. The simplest technique to identify the active voxels is the subtraction technique, in which the average of all the acquired data during the control task are subtracted from the average data of all the images acquired during stimulus task. When the images are subtracted, if there is no activation in the voxel, the signal should subtract out but due to noise there will be a residual difference. It is difficult to distinguish weak activation and a strong physiological fluctuation.

3.4.1.2 The t-test. In this method, the signal values measured from a particular voxel during the task and control periods are treated as two populations. The significant difference between the means of two groups can be assessed using a t-test. The t-statistic for each voxel is calculated and a threshold is selected. The voxels whose t value passes the threshold are considered active and those voxels are displayed in color.

3.4.1.3 Fourier Analysis. In this method, the Fourier transform of the time course is measured and the component at the fundamental frequency of the stimulus pattern is examined. If four cycles of stimulus and control tasks are performed in an experiment, then the amplitude for the 4-cycle frequency in the Fourier spectrum should be a strong spike whenever there is activation. The delay of the response is easily calculated and this is the advantage of this method. The haemodynamic delay is not uniform and it may vary from one part to other. When the standard correlation analysis method is used, there is a problem because the delay used in the model does not match the true delay so the correlation coefficient is reduced. As a result, the activated voxels which should be identifiable are missed. To overcome this problem, the correlation coefficient is calculated for the same model but with different delays and the one that gives the greatest

value of r can be selected as the best fit. If the model response function is a sine wave, then the best fit of the delay can be calculated using Fourier Transform.

3.4.1.4 Correlation Analysis. In this method, the idealized box-car waveform is used a reference waveform. It is assumed that, the reference waveform is a scaled version of the input stimulus. The reference waveform is then correlated with every voxel in the brain and the parameter r ranges from -1 to +1. This value expresses the degree of correlation. A histogram analysis of the correlation coefficient in the brain is computed. All voxels typically greater than a set threshold is considered active and belonging to the task activation regions. After performing correlation, the regions that are colored are the regions that are activated for a given stimulus. The voxels that are not colored imply that they are not activated. It implies that, the statistical quality of measurements in those voxels is too low, so one cannot confidently say there is activation. Activation maps are created using correlation method and these maps are overlaid on anatomical images.

3.4.2 Non-Parametric Methods

In non-parametric methods, the data is not assumed to follow any distribution and they are also called as distribution free methods.

Kolmogorov-Smirnov (KS) test. The statistical significance of the detected activation can be evaluated using the KS test. In this method, the signal values measured during the control and stimulus periods are treated as two populations. With the KS test, the focus is on whether the cumulative distributions of the two populations are significantly different. All signal values are measured in the activated state and are sorted in ascending order. An estimate of the cumulative distribution is formed by calculating P(x), the fraction of signal values x for each x. $P_{act}(x)$ and $P_{rest}(x)$ are the two distributions and the KS statistic

is calculated as the maximum difference between the two cumulative distributions. With the KS test some weak activation can be missed but the ones that are deemed to be significant are likely to be reliable.

3.4.3 Data Driven Methods

The data driven methods explore the fMRI data statistically without any assumption of the paradigm and the advantage is that the unexpected components like drift, motion related artifacts can be detected. The two commonly used data driven methods are Principal Component Analysis and Independent Component Analysis.

3.4.3.1 Principal Component Analysis. Principal component Analysis (PCA) was first introduced by Pearson and is the oldest and best known of the techniques of multivariate analysis [40]. It is a method that reduces dimensionality of the data. In order to examine the relationship among a set of correlated variables, it may be useful to transform the original set of variables to a new set of uncorrelated variables called principal components. These new variables are linear combinations of the original variables and are derived in decreased order of importance so that the first principal component accounts for as much as possible of the variation in the original data [41].

The dataset collected in a functional imaging study can be represented in a matrix X whose dimension is n x p, where n is the number of individual scan images collected as a time series and p is the total number of voxels in the image [42]. For the data matrix X, the covariance matrix is calculated. PCA consists of finding the eigen values and eigen vectors of the covariance matrix of the data matrix X. The eigen vectors are called the principal components and the eigen values give the variance of the corresponding eigen vector [43]. After finding the eigen vectors of the covariance matrix, the vectors are

arranged in order by the eigen values (from highest to lowest). This gives the components in order of significance. The first eigen vector represents the largest source of variation between pairs of voxels and this is the first principal component [31].

The principal components obtained are cross correlated and by selecting appropriate threshold the activation maps are generated.

3.4.3.2 Independent Component Analysis. ICA belongs to class of blind sources separation methods for separating multivariate data into informational components. The problem of unmixing signals is known as blind source separation (BSS) and independent component analysis is a specific method for performing BSS. The term blind is intended to imply that such methods can separate data into source signals even if very little is known is known about the nature of those source signals. [44] The observed fMRI signal is a linear mixture of various signal sources and components originating from the cardiac and respiratory pulsations [45] and the blind source technique can be applied to obtain the independent signal sources.

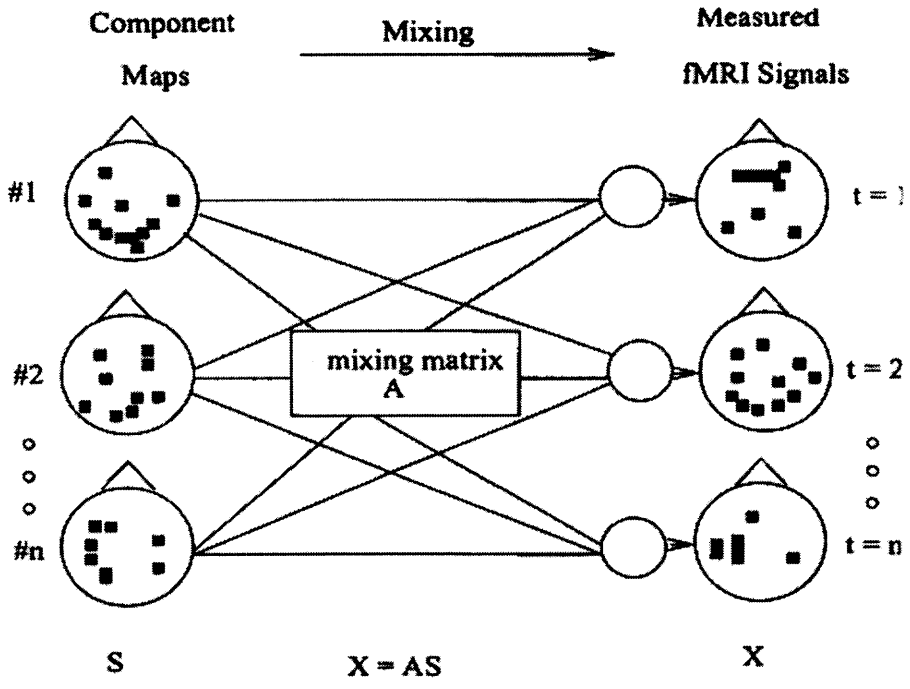

Figure 3.2 fMRI data as a mixture of independent components.

The relationship between the observed voxel time courses and the source signals can be expressed as

$$\mathbf{x}=\mathbf{As} \tag{3.2}$$

Where x is the observed voxel time series

A is the mixing matrix and

s represents the independent source signals

The goal of ICA is to estimate the mixing matrix A so that the source signals can be obtained from the mixture. [46]. The basis for unmixing the source signals from the mixtures in ICA is that, the source signals are statistically independent and the source signals have non-gaussian distribution. In order to estimate the mixing matrix A, x is linearly transformed to a new vector v such that its components are uncorrelated and their

variance equals unity [47] v=Mx. This is called whitening and it should be done before applying any ICA algorithm. v=MAs=Bs where B=MA is an orthogonal matrix .The source signals can be obtained $s= B^T x$. The ICA decomposition of x is given by

$$\mathbf{s=Wx} \tag{3.3}$$

where W is the unmixing matrix and is usually the inverse of mixing matrix A.

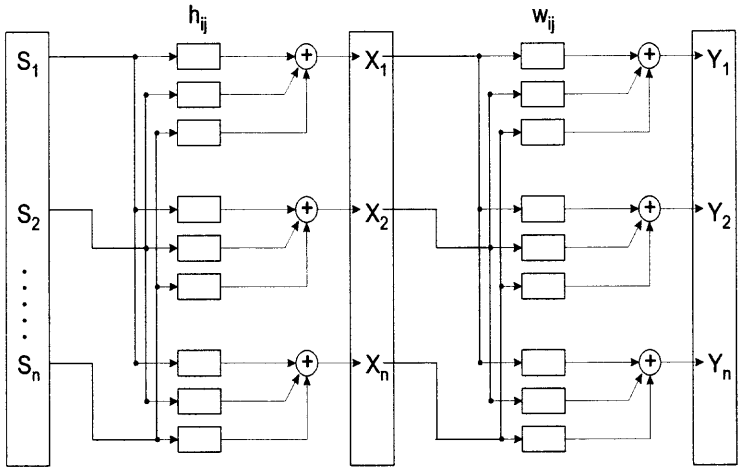

Figure 3.3 Schematic diagram of the blind source separation problem.

In the above figure, $S(t) = [s_1(t), s_2(t), \ldots s_n(t)]$ represents the signal sources which are generally task-induced response, cardiac rate, respiratory rate etc, $X(t) = [x_1(t), x_2(t), \ldots x_n(t)]$ represents the observed voxels time series, h_{ij} is the unknown mixing matrix, W_{ij} is the unmixing matrix. The signal sources S(t) and the mixing matrix h_{ij} are unknown. The aim is to find $Y(t) = [y_1 (t), y_2 (t), \ldots y_n(t)]$ without knowing the signal sources and the mixing matrix and is achieved using blind source separation technique.[45].

The algorithms used for finding ICA are infomax [48], FastICA [46], Joint Approximate Diagnolization of Eigen matrices [49] etc. In this study FastICA algorithm was used and is discussed briefly here.

FastICA algorithm. FastICA learning rule finds a direction such that the projection W^T x maximizes non-guassianity. Non-guassianity in this algorithm, is measured by the approximation of negentropy J (W^Tx). Fast ICA is based on a fixed point iteration scheme for finding a maximum of the non-guassianity of W^Tx. [47]. The number of components determined by any ICA algorithm is equal to the number of time points in the input data.

The independent components obtained from the algorithm are cross correlated with all the voxels and a threshold value is selected. The voxels that pass this threshold are considered active and activation maps are generated.

Summary

This chapter provided an overview of Functional Magnetic Resonance Imaging (fMRI). The response of the brain to a particular stimulus is measured using Blood Oxygenation Level Dependent (BOLD) mechanism. The least square algorithm is implemented in AFNI for registering images and this algorithm was used in this study. Different methods for detecting active voxels are discussed in this chapter and the techniques namely Cross correlation, Independent Component Analysis and Principal Component Analysis was used in this study for determining the active voxels.

CHAPTER 4

MATERIALS AND METHODS

4.1 Data Acquisition

Four autistic subjects and eight healthy matched controls were recruited for this study. Written informed consent was obtained from all the subjects according to the guidelines established by the Institutional Review Board at UMDNJ. Four subjects were diagnosed with autism as measured on the AD1-R (Autism Diagnostic Interview – Revised [50]), the ADOS-G (Autistic Diagnostic Observation Schedule – Generic [51]) and the DSM-IV (Diagnostic and Statistical Manual [52]). The diagnosis was done by Dr. Charles Cartwright.

Autistic subjects were recruited from Dr.Cartwright's clinical consultation at the Autism and Anxiety Disorder programs (UMDNJ Newark). Data were collected using the 1.5 T GE scanner. Subjects were placed in the gantry and the surface coil was positioned over their head. The subjects were positioned in the MRI gantry with their head placed along the mid-sagital plane. The subjects were instructed to keep their head still. Foam padding was used to minimize head motion. Each session began with the acquisition of high resolution anatomical images. High resolution anatomical images were acquired in axial planes for the use of anatomical landmarks and registration purposes with 28 slices at 5mm thickness, FOV = 240 mm and the matrix size was 256x256 mm. For functional runs, several time series of echo planar images were obtained using a T2* weighted gradient echo pulse sequence. The imaging parameters included a matrix size of 64x64 mm2, FOV of 240 mm, 28 slices each 5mm thick. Other imaging parameters included TR of 1000 msec, and TE of 40 msec.

Control subjects data were collected using 3 T Allegra scanner. Anatomical images were acquired with 11 slices covering the entire sensory motor cortex, FOV = 240 mm and the matrix size was 256x256 mm. For functional images, 11 axial slices were obtained using a T2* weighted gradient echo pulse sequence with TR = 1000ms, FOV=240 mm and the matrix size was 64x64 mm.

4.2 Experimental Task

A motor task paradigm was used for this study. Subjects were instructed to perform a bilateral finger tapping for a period of time with alternating period of rest. Subjects tapped their fingers (in both hands) using the periodic scanner noise as the auditory cue. Typically, the finger tapping rate varied between 0.5 to 2 Hz. A typical reference waveform representing the ON/OFF cycle of the finger tapping task is shown below:

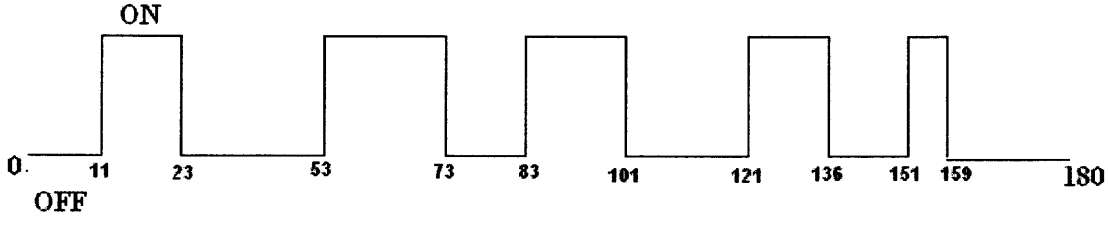

Figure 4.1 Reference waveform.

4.3 Data Analysis

The data for this study were analyzed using AFNI. [53]. The first five time points of each time series corresponding to the first 5 s of data acquisition for T_1 relaxation were discarded from the beginning for each series.

4.3.1 Motion Correction

Because the motion was a concern particularly in children with autism, all datasets obtained from all the subjects were tested for the presence of any head induced signal change. Head motion causes spurious signal changes in the brain and makes detection of activation signal difficult. Thus, while activation induced signal changes by about 5%, head motion induced signal changes can be as high as 50% above the mean. Head motion not only reduces the signal to noise ratio in the activated regions but also produces spurious activations, especially at borders at the edge of the brain and between large fissures. In order to reduce the artifact due to motion, it is necessary to register the images. Image registration refers to the process of aligning time series of MR images to minimize the effect of movement. Registration reduces the effective noise level and increase the number of detected activations. The fMRI images of all the subjects were registered in AFNI. The algorithm used in AFNI is iterative linearized weighted least squares [54] and in this algorithm, each sub brick from the input data is registered to the base brick.

4.3.2 Automatic Detection of Task-Activation

Although a large number of data analysis methods currently exist, each of them make certain assumptions regarding the nature of the experiment. One of the assumptions made is that, the experimenter knows the exact sequence of stimulus being presented i.e., input function. While for a number of cases it is true, for a number of cases it cannot be assumed to be true. For example, while an elderly subject with Alzheimers (or children with autism) may not be able to follow the task for the entire duration and may even forget the task being done. For certain task paradigm, it is also possible that the response (example, drug response involving pharmacokinetic studies) is not linear. For cases like these, correlation (for example) would lead to difficulty in detecting results since the input stimulus is not similar to the way in which the subject performed the task.

In this method developed, the assumption made is that the activation typically involves larger region comprising of several voxels and that these neighboring activated voxels are also temporally correlated. One problem with this assumption is that, vessels and CSF pulsations (typically unrelated to the task) also are spatially located and temporally have high degree of correlation. However, the primary distinction in the signal characteristics between the signals from large vessels and that from task-activation signal changes is that because the vessels have relatively higher frequency components caused predominantly by respiration. Typical respiration rate is about 12-15 cycles per minute. To minimize the effect of large vessel and CSF, the reference vector is shifted several time points in an incremental fashion and correlation performed during each step. Because the respiration frequency is significantly faster compared to the task-induced

response, the mean correlation coefficient decreases much quicker than that obtained by shifting the task response. Typically, 4 time points (8 sec) was found to be adequate to cover more than one complete respiration cycle, while only covering half a cycle of task presentation. The mean correlation from vessels and the cerebro spinal fluid (CSF) would be less that that from activated voxels. A simple threshold method was then used to identify voxels with high mean correlation-coefficient across several time shifts and threshold applied.

This process can be implemented using the following steps:

- Correlating every voxel time series in the brain with the time series of its neighboring voxels (either 8 or 4).
- Shifting the center (reference) time series by one time point and the correlation coefficient with its neighbors is calculated. Typically, this is repeated 4 times and mean correlation coefficient determined.
- This is performed for every voxel in the brain.
- A threshold is used to identify the activated regions of the brain.

All the four steps were implemented in AFNI. Each voxel time series was treated independently and the linear and quadratic trend was removed from the time series using least squares. A binary mask was created on the input dataset using an intensity voxels in the brain. The time series of a voxel was correlated with the time series of its neighboring voxels and the mean correlation coefficient was calculated.

4.3.3 Analysis using Cross Correlation Method

Task activated voxels were determined using cross correlation method and in this method, the reference waveform representing the ON/OFF cycle of the finger tapping task was cross-correlated with all the voxels on voxel- by-voxel basis and a threshold

was used to generate the activation maps. All voxels whose intensity values passed the threshold were considered active.

4.3.4 Analysis using PCA

In this method, a binary mask was first created with a threshold 0.2. The principal components of the selected voxels time series were obtained in AFNI. Five principal components were obtained and the component whose pattern matched the voxel time series was selected and cross correlated. A threshold was used and the voxel values that passed the threshold were considered active and activation maps were generated.

4.3.5 Analysis using ICA

The voxels time series were extracted from the input dataset that satisfied the mask criterion. After extracting the time series of the desired voxels, the FastICA algorithm was used to determine the independent components. Five independent components were obtained and the component whose pattern matched the voxel time series was selected and cross correlated. The voxels intensity values that passed the threshold were considered active and activation maps were generated.

CHAPTER 5

RESULTS

5.1 Introduction

This chapter discusses the results obtained in this study. For the given bilateral finger tapping stimulus, the active voxels belonging primarily in the sensorimotor cortex region were identified The results were obtained using the automatic detection method, correlation method, Independent Component Analysis, Principal Component Analysis.

5.2 Motion Corrected Data

A least square weighted algorithm was used to correct the motion artifacts for all the subjects. The goal of the algorithm is to align the target image with a reference image which was typically chosen from the series. To align the target image with the reference image, the target image was translated and rotated. The new image matrix is an appropriate interpolation of the original image onto the new registered grid. For this study, head induced signal changes was found to be minimal. The mean shift in images was found to be less than 0.1. In all the subjects across all the runs, the motion estimates were found to be less than the set value of 2 pixels, and thus all the data sets were used for further analysis.

5.3 Detection of Activated Voxels

The active voxels in the motor cortex region was detected automatically. The preprocessing step was to detrend the voxels time series. All voxels from the brain was used to perform correlation with its neighbors and its mean correlation coefficient between its surrounding voxels was determined. The activation maps were generated and a threshold of 0.24 was used for normal subjects and a threshold of 0.21 was used for autistic subjects.

The cross-correlation images were obtained by cross correlating the reference waveform with every voxel time course on a voxel-by-voxel basis in the fMRI image. The activation map was generated with a mean correlation coefficient threshold of 0.55 for normal subjects and 0.49 for autistic subjects.

To validate the results obtained using the automatic correlation method, PCA and ICA was also performed on the detected voxels. Five dominant components were determined across each of the methods for all the subjects.

In PCA, the voxels time courses from the datasets that satisfied the mask criterion were extracted and five components were obtained. The first component was selected as reference. The time course of the selected component was correlated on a voxel –by-voxel basis with every voxel time course. A threshold of 0.77 was obtained for normal subjects and a threshold of 0.59 was obtained for autistic subjects and activation maps were generated.

In ICA also, the time series of the voxels were extracted from the input datasets that satisfied the mask criterion. The independent components were obtained using FastICA algorithm in MATLAB. ICA derived only one component that matched the

voxels time series and it was selected as the reference. Activation maps were obtained by correlating the time course of the selected component with the voxels time course. For normal subjects, a threshold of 0.78 was obtained and for autistic subjects a threshold of 0.58 was obtained.

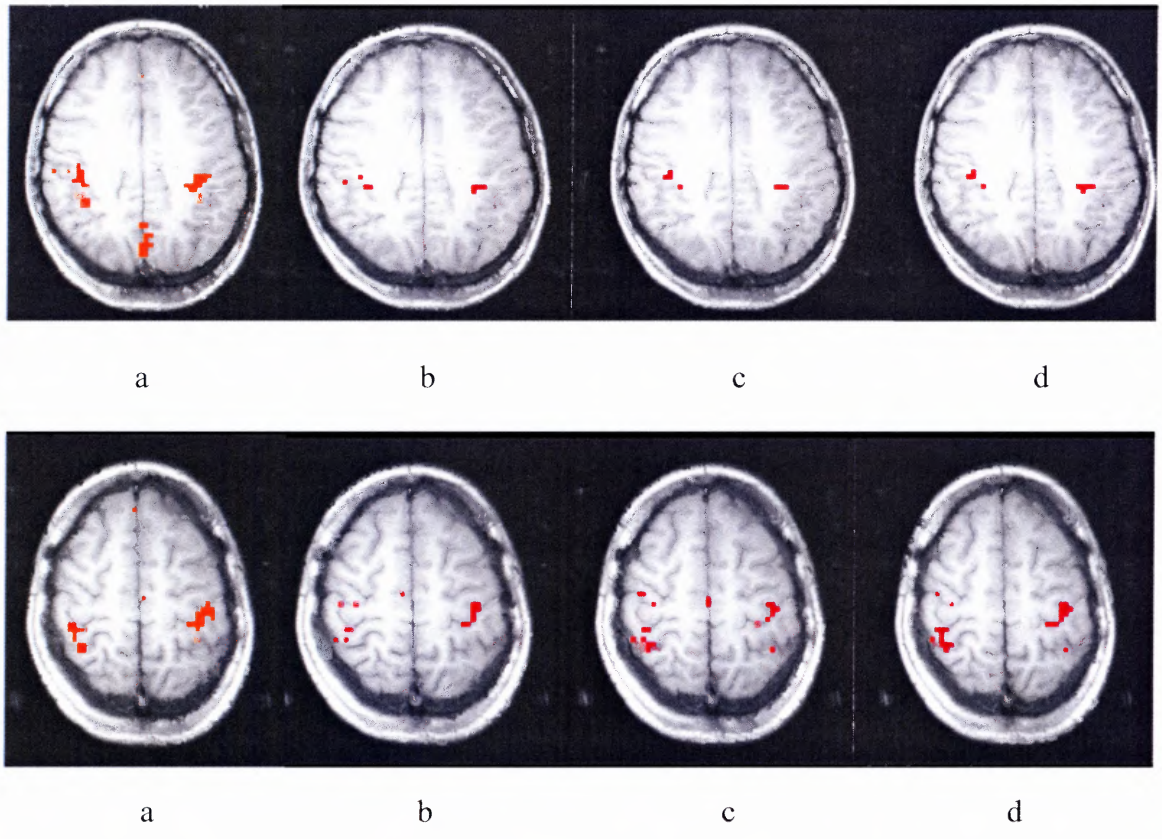

Figure 5.1 Images obtained during the finger tapping paradigm and the images are obtained by a. Automatic detection b. Correlation c. Principal Component Analysis and d. Independent Component Analysis methods. The first four images are from Normal Subject # 6 (Slice # 9) and the last four images are also from the same subject (Slice # 10).

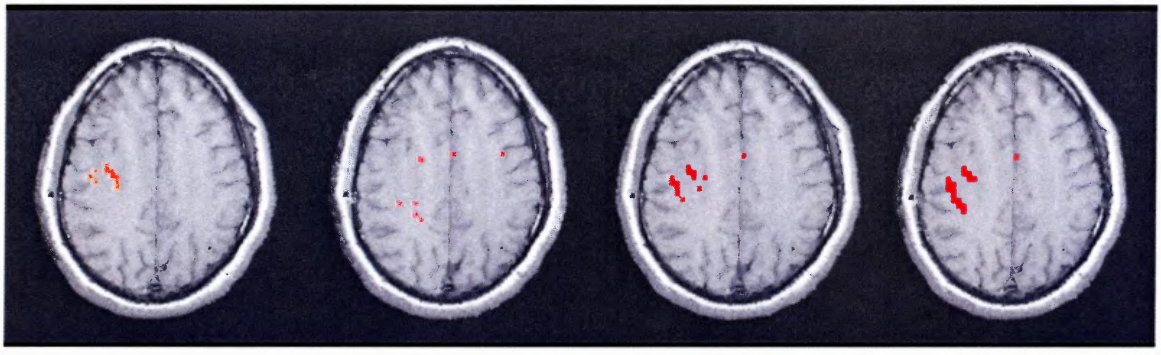

a b c d

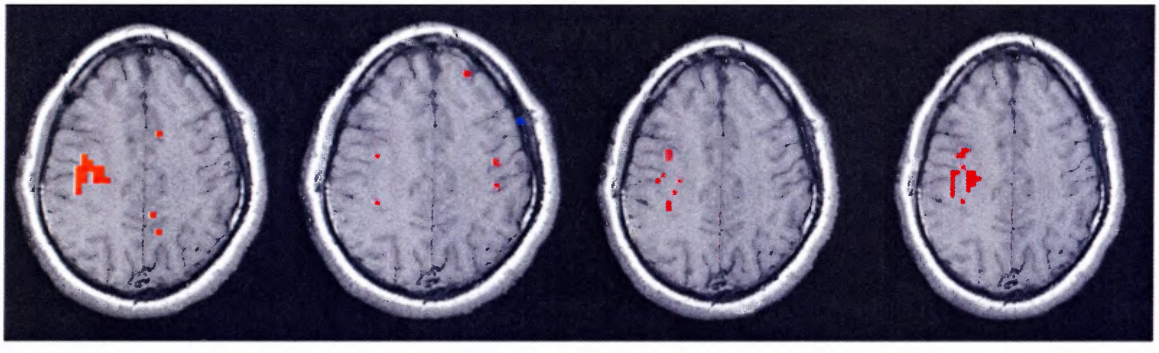

a b c d

Figure 5.2 Images obtained during the finger tapping paradigm and the images are obtained by a. Automatic Detection b. Correlation c. Principal Component Analysis and d. Independent Component Analysis methods. The first four images are from Autistic Subject # 1 (Slice # 22) and the last four images are also from the same subject (Slice # 23).

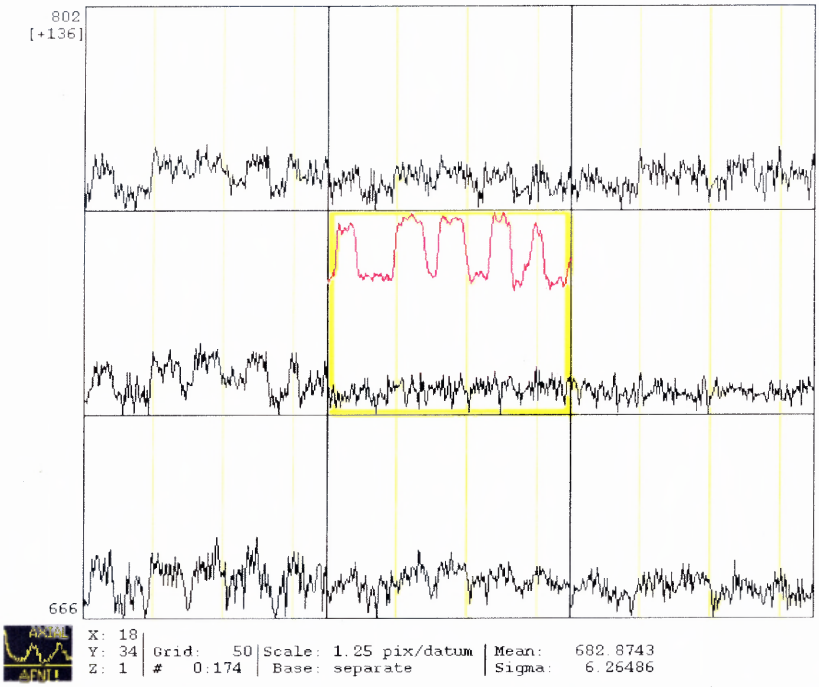

Figure 5.3a BOLD signal obtained from the finger tapping paradigm from Normal subject # 6. The waveform in red is the first independent component.

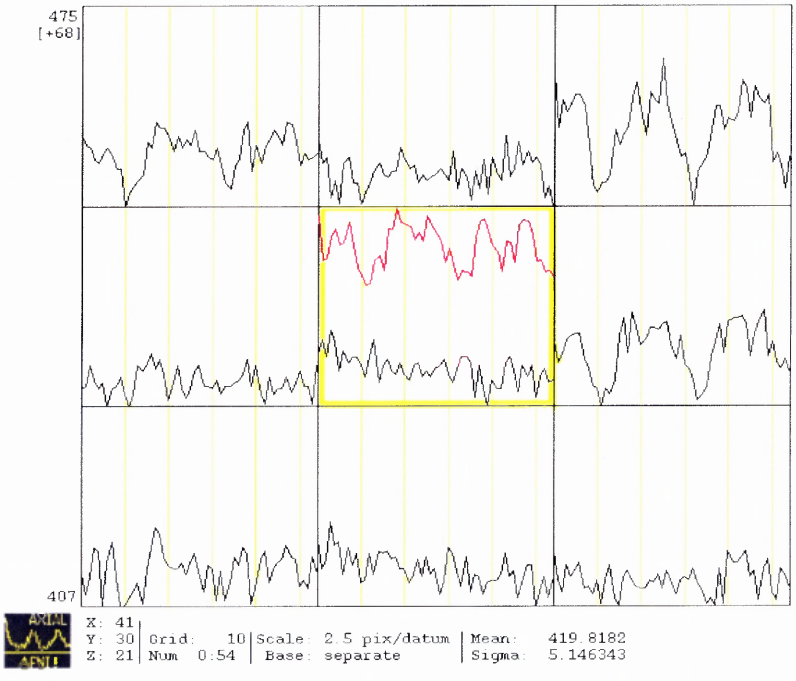

Figure 5.3b BOLD signal obtained from the finger tapping paradigm from Autistic subject # 1. The waveform in red is the second independent component.

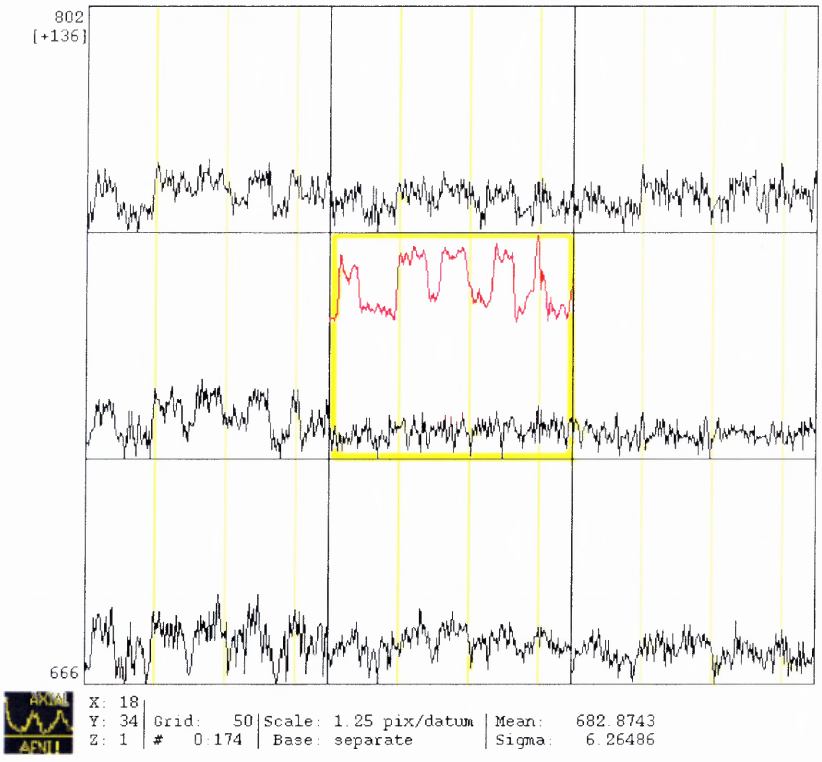

Figure 5.4a BOLD signal obtained from the finger tapping paradigm from Normal subject # 6. The waveform in red is the first principal component.

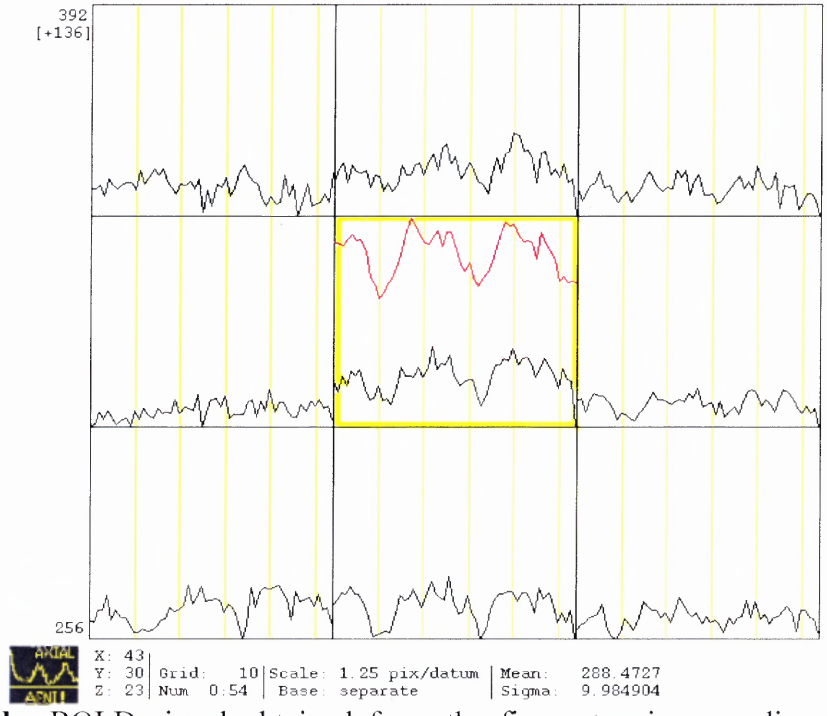

Figure 5.4b BOLD signal obtained from the finger tapping paradigm from Autistic subject # 1. The waveform in red is the first principal component.

In this study, a method for detecting activated voxels without using prior knowledge of the input stimulus was presented. To validate the accuracy of this method, comparisons were made by using PCA and ICA analysis. A significant overlap in the sensorimotor cortex was found between the various methods suggesting the automatic detecting method presented here does provide accurate detection and localization.

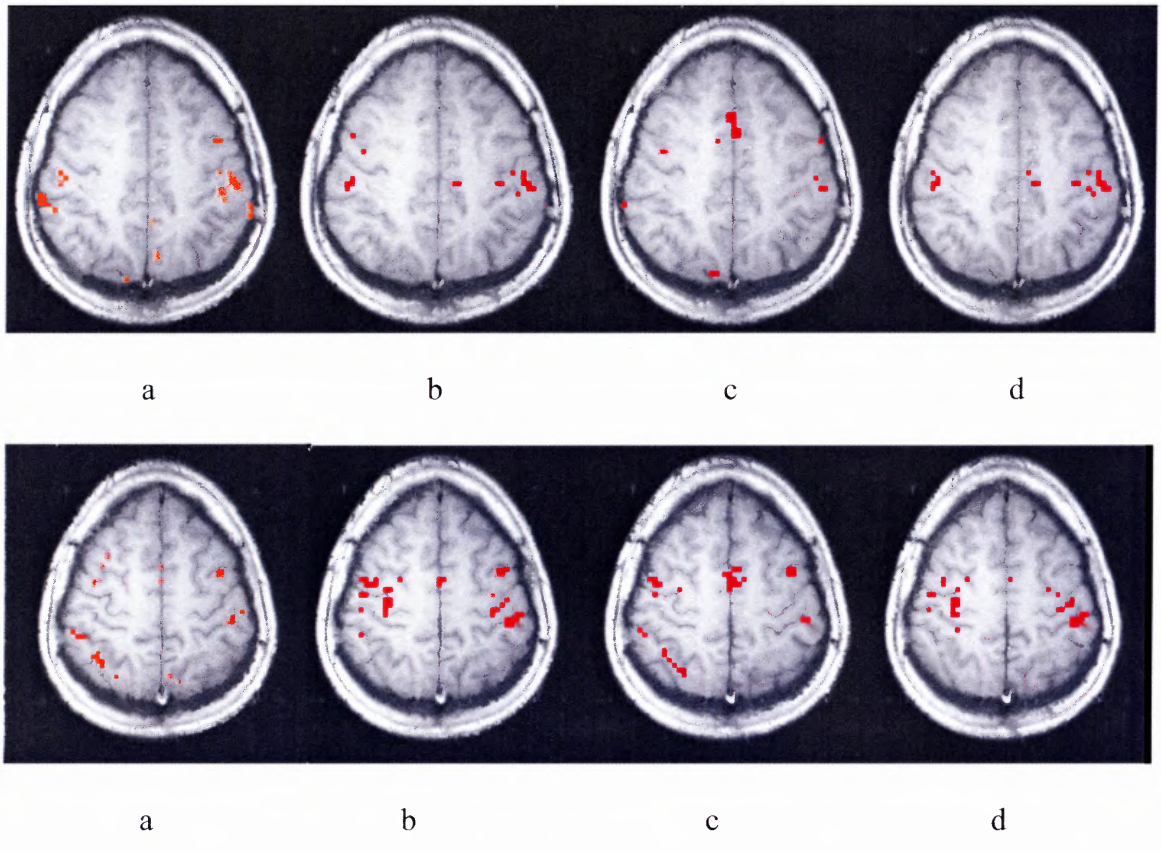

Figure 5.5 Images obtained during the finger tapping paradigm and the images are obtained by a. Automatic Detection b. Correlation c. Principal Component Analysis and d. Independent Component Analysis methods. The first four images are from Normal Subject # 2 (Slice # 8) and the last four images are also from the same subject (Slice # 9).

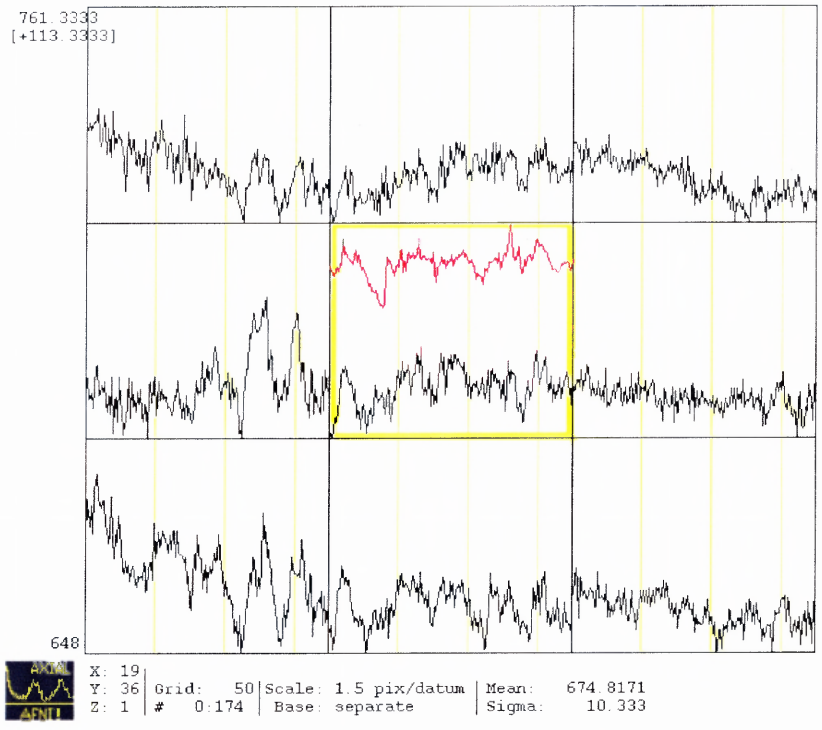

Figure 5.6a BOLD signal obtained from the finger tapping paradigm from Normal subject # 2. The waveform in red is the second independent component.

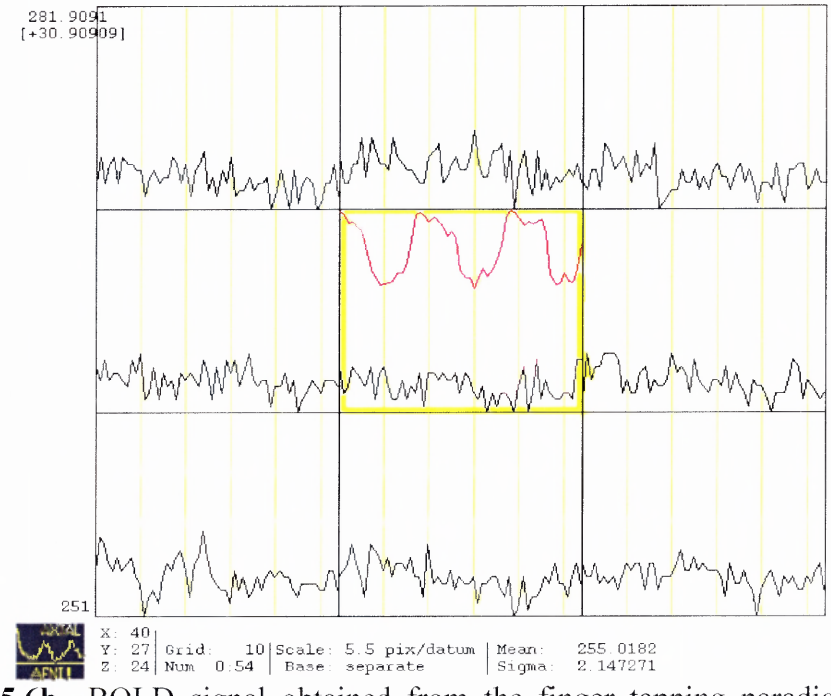

Figure 5.6b BOLD signal obtained from the finger tapping paradigm from Autistic subject # 5. The waveform in red is the first independent component.

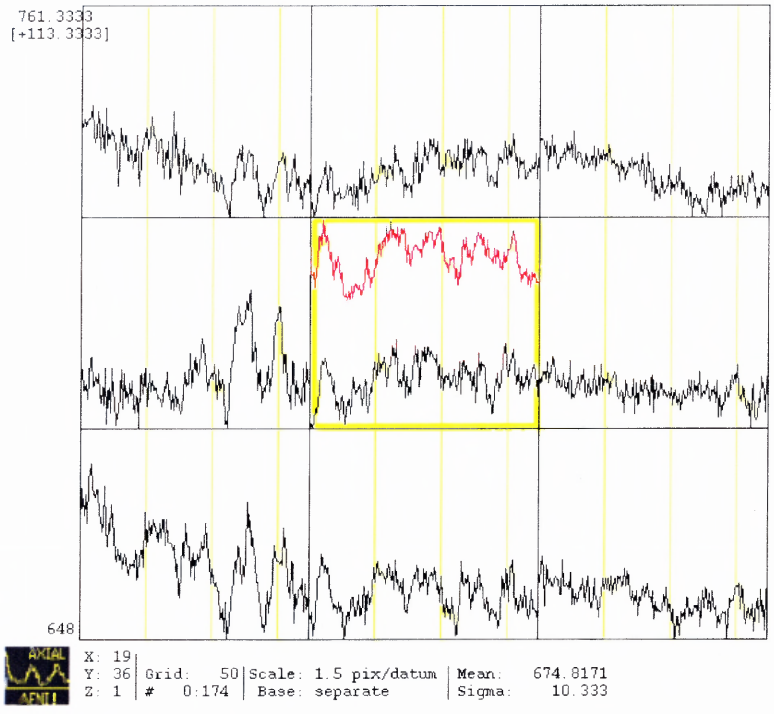

Figure 5.7a BOLD signal obtained from the finger tapping paradigm from Normal subject # 2. The waveform in red is the first principal component.

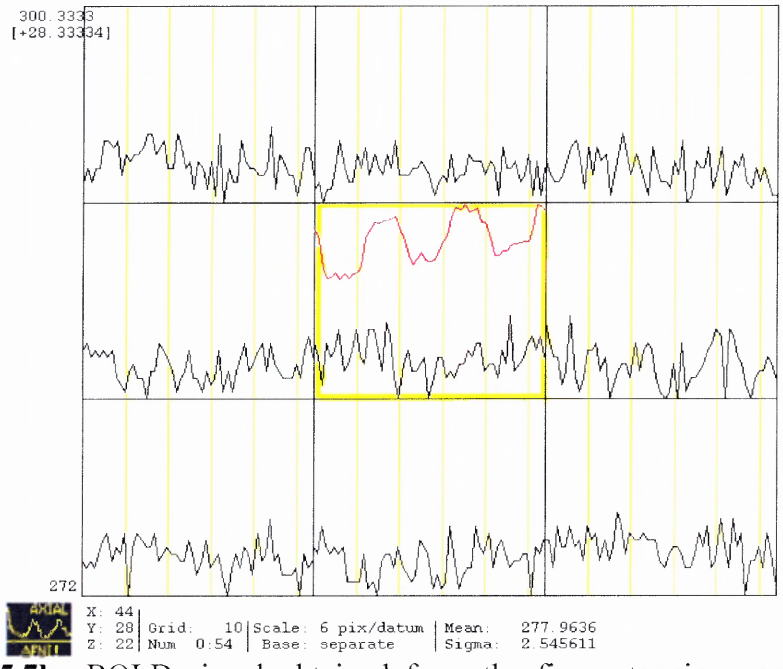

Figure 5.7b BOLD signal obtained from the finger tapping paradigm from Autistic subject # 5. The waveform in red is the first principal component.

Figure 5.3a, 5.4a, 5.6a and 5.7a represents the time course of the voxels in the motor cortex region for the normal subjects and 5.3b, 5.4b, 5.6b and 5.7b represents the time course of the voxels in the motor cortex region for autistic children. Both PCA and ICA, extracted the component that contained the task-induced response. The correlation coefficient threshold for both PCA and ICA was high which implies that the pattern of the principal and independent component and the pattern of the voxels time series matched well.

CHAPTER 6

DISCUSSION AND CONCLUSION

Functional magnetic resonance imaging is the fast emerging as the tools for studying the brain function due to its non-invasiveness in addition to high spatial and temporal function. Changes in cerebral metabolism, blood flow volume or oxygenation in response to a task can be detected and localized. Currently, both human and animal studies are used to localize changes in cerebral blood flow, oxygenation. A number of clinical population studies are currently being done. Several clinical studies including preoperative surgical mapping has almost become standard clinical practice.

Although a large number of data analysis packages exist, no standard procedure or even a sequence of procedure exists to facilitate researchers with analyzing datasets. Clearly, the statistical analysis of the blood oxygenation level data is the critical part. The images have to be pre-processed prior to statistical analysis so that noise level is reduced and the signal to noise ratio is increased. The commonly used pre-processing steps are image registration, filtering and smoothing.

The commonly used techniques for fMRI data analysis are cross-correlation technique, t-test and general linear model. These techniques are easy to implement and are effective but cannot be applied when the neural response is complicated and also when fMRI response is unknown. Also in the above methods, the noise level is assumed to be same for all the voxels and the active voxels detected by these methods are less reliable.

The active regions can be detected reliably without assuming any model for the fMRI response. Principal Component Analysis and Independent Component Analysis are

the two commonly model free methods used for analyzing the fMRI data. In both the methods, the original data is transformed to a high dimensional vector space so that the functional response can be separated from various noise sources. The difference between PCA and ICA is that, PCA separates the signal sources that are uncorrelated and ICA separates the signal sources that are independent. PCA cannot accurately the task induced response as ICA so PCA is generally used for reducing the dimension of the original data.

The Biasless Identification of Activated Sites by Linear Evaluation of Signal Similarity (BIASLESS) technique proposed by Levin is based on the assumption that the time course of the signals in activated voxels will not vary when the task is repeated by the same individual. Even though the method is simple and model independent, it cannot be used in situations where the subjects have to perform different tasks.

Many potential advantages exist with using automatic detection of task-induced signal response without initially using the reference waveform. One is able to determine the various clusters of activations that exist in the brain. This is particularly important if the subject being scanned is not able to follow the task or the subject's performance changed during the task. Further analysis including PCA or ICA can then be performed on those voxels to further analyze the activation and signal response. This substantially constrains the search of the PCA and ICA algorithms. ICA or PCA is done on the whole brain in addition to being computationally expensive. It also does not guaranty that the activation response will be the first component.

Habituation and learning effects can also be seen via this method. Through automated analysis, areas of the brain solely associated with the event or task will be shown if the stimulus is randomized. If this type of stimuli is administered along with a

highly repetitive action, regions associated with habituation or learning will be active when compared to the randomized period. More can be learned about the brain and its habituation and learning functions via this type of experiment.

With event related M-sequence, fMRI studies are increasingly being used in neuroscience research to detect hemodynamic responses associated with transient brain activation. It can detect regions of the brains that are associated with a particular sensory, motor, or cognitive task. For these kind of studies, automated analysis is ideal. The ability to randomize the length of the event or task also offers the ability to narrow down which regions of the brain are involved with certain tasks or events. With the ability to randomize the task or event, distinct regions of the brain can be more clearly seen.

Regions of the brain with high physiological noise component can also be seen through the method developed. In certain regions, for example near the sagital sinus regions associated with the cardiac and respiration frequency can be seen.

This technique also allowed for a novel experiment paradigm that randomized the ON-OFF time lengths of finger tapping. This paradigm can be modeled for stimuli that may need various different time lengths or are unpredictable before the time of the study. The experiment undertaken was a simple finger-tapping paradigm yet regions of activation were visible in accordance with the reference stimuli waveform.

With the automated detection method, there are also limitations. This method assumes that the activation occurs in a number of neighboring voxels, and that these voxels have similar temporal patterns. It is however possible that some tasks can be designed that activates only a few voxels (less than 4 voxels).

This study used a new method to detect the active voxels in the brain. The assumption made is that the activation involves large number of regions and the neighboring activated voxels are temporally correlated. Using this method, activation maps were generated and to validate the results Principal Component Analysis and Independent Component Analysis were also performed. Analysis of the results revealed that the automatic method can be used to reliably detect the activated voxels. Also, the active voxels can be detected without using prior knowledge of the reference waveform.

Although PCA and ICA was used in this thesis for analysis, other time-domain methods such as t-test, F-test, etc., frequency-domain methods such as Fourier analysis, or time-frequency domain methods can be used to further analyze the data sets.

A simple finger tapping paradigm was used for this study. For individual paradigms like text listening, face processing, paradigms that stimulates the visual cortex and also for multiple paradigms, the automatic method can be employed to detect the active voxels. A randomized block design was considered for this study and it can be further extended to the event related design.

Functional connectivity exists in the resting brain and it has been reported in motor regions, auditory regions, language system and visual regions of the brain. The automatic method used in this study can be applied to detect the functional connectivity of the brain in the resting state.

REFERENCES

1. L. Wing and D. Potter, "The Epidemiology of the Autism Spectrum Disorders: Is the prevalence rising?," *Mental Retardation and Developmental Disabilities Research Reviews"*, vol. 8, pp. 151-161, 2002.

2. H. H. Bartholomeusz, E. Courchesne, and C. M. Karns, "Relationship between head circumference and brain volume in healthy normal toddlers, children, and adults," *Neuropediatrics*, vol. 33, pp. 239-241, 2002.

3. M. Conciatori, C. J. Stodgell, S. L. Hyman, M. O'Bara, R. Militerni, C. Bravaccio, S. Trillo, F. Montecchi, C. Schneider, R. Melmed, M. Elia, L. Crawford, S. J. Spence, L. Muscarella, V. Guarnieri, L. D'Agruma, A. Quattrone, L. Zelante, D. Rabinowitz, T. Pascucci, S. Puglisi-Allegra, K. Reichelt, P. M. Rodier, and A. M. Persico, "Association between the HOXA1 A218G polymorphism and increased head circumference in patients with autism," *Biological Psychiatry*, vol. 55 (4), pp. 413-419, 2004.

4. S. D. Friedman, D. W. Shaw, A. A. Artru, T. L. Richards, J. Gardner, G. Dawson, S. Posse, and S. R. Dager, "Regional brain chemical alterations in young children with autism spectrum disorder," *Neurology*, vol. 60 (1), pp. 100-107, 2003.

5. J. G. Levitt, J. O'Neill, R. E. Blanton, S. Smalley, D. Fadale, J. T. McCracken, D. Guthrie, A. W. Toga, and J. R. Alger, " Proton magnetic resonance spectroscopic imaging of the brain in childhood autism," *Biological Psychiatry*, vol. 54 (12), pp. 1355-1366, 2003.

6. H. Otsuka, M. Harada, and K. Mori, "Brain metabolites in the hippocampus – amygdala region and cerebellum in autism: a 1H-MR spectroscopy study," *Neuroradiology*, vol. 41, pp. 517-519, 1999.

7. D. C Chugani, B. S. Sundaram, and M. Behen, "Evidence of altered energy metabolism in autistic children," *Prog. Neuropsychopharmacol Biol Psychiatry*, vol. 23, pp. 635-641, 1999.

8. N. Akshoomoff, K. Pierce, and E. Courchesne, "The neurobiological basis of autism from a developmental perspective," *Development and psychopathology*, vol. 14, pp. 613-634, 2002.

9. E. Courchesne, C. M. Karns, H. R. Davis, R. Ziccardi, R. A. Carper, Z. D. Tigue, H. J. Chisum, P. Moses, K. Pierce, C. Lord, A. J. Lincoln, S. Pizzo, L. Schreibman, R. H. Haas, N. A. Akshoomoff, and R. Y. Courchesne, "Unusual brain growth patterns in early life in patients with autistic disorder: An MRI study," *Neurology*, vol. 57 (2), pp. 245-254, 2001.

10. T. Hashimoto, M. Tayama, K. Murakawa, T. Yoshimoto, M. Miyazaki, M. Harada, and Y. Kuroda, "Development of the brainstem and cerebellum in autistic patients," *Journal of Autism and Developmental Disorders*, vol. 25, pp. 1-18. 1995.

11. J. G. Levitt, R. Blanton, L. Capetillo-Cunliffe, D. Guthrie, A. Toga, and J. T. McCracken, "Cerebellar vermis lobules VIII - X in autism," *Progress in Neuro-Psychopharmacology and Biological Psychiatry*, vol. 23 (4), pp. 625-633, 1999.

12. O. Koul, "Myelin and Autism", Paper presented at the International meeting for Autism Research, San Diego, CA, 2001.

13. T. L. Kemper, M. Bauman, "Neuropathology of infantile Autism," *Journal of Neuropathology and Experimental Neurology*, vol. 57 (7), pp. 645-652, 1998.

14. R. A. Carper, P. Moses, Z. D. Tigue, and E. Courchesne, "Cerebral lobes in autism: Early hyperplasia and abnormal age effects," *NeuroImage*, vol. 16 (4), pp. 1038-1051, 2002.

15. M. F. Casanova, D. P. Buxhoeveden, A. E. Switala, and E. Roy, "Minicolumnar pathology in autism," *Neurology*, vol. 58 (3), pp. 428-432, 2002.

16. F. Abell, M. Krams, J. Ashburner, R. Passingham, K. Friston, R. Frackowiak, F. Happé, C. Frith, and U. Frith, "The neuroanatomy of autism: A voxel-based whole brain analysis of structural scans," *NeuroReport*, vol. 10 (8), pp. 1647-1651, 1999.

17. L. Waterhouse, D. Fein, C. Modahl, "Neurofunctional mechanisms in autism," *Psychological Review*, vol. 103 (3), pp. 457-489, 1996.

18. K. B. Nelson, J. K. Grether, L. A. Croen, J. M. Dambrosia, B. F. Dickens, L. L. Jelliffe, R. L. Hansen, and T. M. Phillips, "Neuropeptides and neurotrophins in neonatal blood of children with autism or mental retardation," *Annals of Neurology*, vol. 49 (5), pp. 597-606, 2001.

19. M. E. Morrison and C. A. Mason, "Granule neuron regulation of purkinje cell development: striking a balance between neurotrophins and glutamate signaling," *Journal of Neuroscience*, vol. 18, pp. 3563-3573, 1998.

20. P. M. Rodier, "The early origins of autism," *Scientific American,* vol. 282, pp. 56-63, 2000.

21. R. Müller, N. Kleinhans, N. Kemmotsu, K. Pierce, and E. Courchesne, "Abnormal variability and distribution of functional maps in autism: An fMRI study of visuomotor learning," *American Journal of Psychiatry*, vol. 160, pp. 1847-1862, 2003.

22. G. Allen, E. Courchesne, "Differential effects of developmental cerebellar abnormality on cognitive and motor functions in the cerebellum: An fMRI study of autism," *American Journal of Psychiatry*, vol. 160 (2), pp. 262-273, 2003.

23. S. Baron-Cohen, H. A. Ring, E. T. Bullmore, S. Wheelwright, C. Ashwin, and S. C. R. Williams, "The amygdala theory of autism," *Neuroscience and Biobehavioral Reviews*, vol. 24 (3), pp. 355-364, 2000.

24. N. Hadjikhani, C. F. Chabris, R. M. Joseph, J. Clark, L. McGrath, I. Aharon, E. Feczko, H. Tager-Flusberg, and G. J. Harris, " Early visual cortex organization in autism: an fMRI study," *NeuroReport*, vol. 15 (2), pp. 267-270, 2004.

25. B. Luna, N. J. Minshew, K. E. Garver, N. A. Lazar, K. R. Thulborn, W. F. Eddy, and J. A. Sweeney, "Neocortical system abnormalities in autism: An fMRI study of spatial working memory," *Neurology,* vol. 59, pp. 834-840, 2002.

26. A. Bailey, P. Luthert, A. Dean, B. Harding, I. Janota, M. Montgomery, M. Rutter, and P. Lantos, "A clinicopathological study of autism," *Brain*, vol. 121, pp. 889-905, 1998.

27. M. Bauman and T. Kemper, "The Neurobiology of Autism," *Johns Hopkins University Press*, 1994.

28. I. Rapin, R. Katzman, "Neurobiology of autism," *Annals of Neurology*, vol. 43 (1), pp. 7-14, 1998.

29. P. A. Bandettini, A. Jesmanowicz, E. C. Wong and J. S Hyde, "Processing Strategies for Time-Course Data Sets in Functional MRI of the Human Brain," *Magnetic Resonance in Medicine*, vol. 30, pp. 161-173, 1993.

30. J. R. Moeller, and S. C Strother, "A regional covariance approach to the analysis of functional patterns in positron emission tomographic data," J.Cereb Blood Flow Metab, vol. 11, pp. A121-A135, 1991.

31. M. J. McKeown, S. Makeig, G. G. Brown, T. Jung, S. S. Kindermann, A. J. Bell, and T. J. Sejnowski, "Analysis of fMRI data by blind separation into independent spatial components," *Human Brain Mapping*, vol. 6 (3), pp. 160-188, 1998.

32. D. N. Levin, and S. J. Uftring, "Detecting Brain Activation in fMRI data without prior knowledge of Mental Event Timing," *NeuroImage*, vol. 13 (1), pp. 153-160, 2001.

33. S. A. Huettel, A.W. Song and G. McCarthy, "Functional Magnetic Resonance Imaging," *Sinauer Associates*, 2004.

34. R. B. Buxton "Introduction to Functional Magnetic Resonance Imaging," Cambridge *University Press*, 2002.

35. J. T. Bushberg, J. A. Seibert, E. M. Leidholdt, J. M. Boone, "The Essential physics of Medical Imaging," *Williams and Wilkins*, 2002.

36. C. Westbrook, and C. Roth, "MRI in practice," *Blackwell Publishing Ltd.*, 1998.

37. J. V. Hajnal, N. Saeed, E. J. Soar, A. Oatridge, I. R. Young, and G. M. Bydder, "A registration and interpolation procedure for subvoxel matching of serially acquired MR images," *Journal of Computer Assisted Tomography*, vol. 19 (2), pp. 289-296, 1995.

38. R. P. Woods, S. R. Cherry, and J. C. Mazziotta, "Rapid automated algorithm for aligning and reslicing PET images," *Journal of Computer Assisted Tomography*, vol. 16 (4), pp. 620-633, 1992.

39. T. D. Otto, A. Meyer-Bäse, M. Hurdal, D. W. Sumners, A. Wismüller, and D. Auer, "Model-free functional MRI analysis using transformation-based methods," *Proceedings of SPIE - The International Society for Optical Engineering*, vol. 5102, pp. 156-167, 2003.

40. I. T. Jolliffe, "Principal Component Analysis," *Springer-Verlag*, New York, 1986.

41. C. Chatfield and A. J. Collins, "Introduction to Multivariate Analysis," *CRC Press*, 1981.

42. A. H. Andersen, D. M. Gash and M. J. Avis, "Principal component analysis of the dynamic response measured by fMRI: a generalized linear systems framework," *Magnetic Resonance Imaging*, vol. 17 (6), pp. 795-815, 1999.

43. G. Zuendorf, N. Kerrouche, K. Herholz and J. C. Baron, "Efficient Principal Component Analysis for Multivariate 3D Voxel-Based Mapping of Brain Functional Imaging Datasets as Applied to FDG-PET and Normal Aging," *Human Brain Mapping*, vol. 18, pp. 13-21, 2003.

44. J. V. Stone, "Independent Component Analysis A tutorial Introduction," *MIT press*, 2004.

45. B. Biswal, and J. Ulmer, "Blind source separation of multiple signal sources of fMRI data sets," *NeuroImage*, vol. 9 (6 PART II), pp. s55, 1999.

46. A. Hyvärinen, and E. Oja, "A Fast Fixed-Point Algorithm for Independent Component Analysis," *Neural Computation*, vol. 9 (7), pp. 1483-1492, 1997.

47. A. Hyvärinen, and E.Oja, "Independent component analysis: Algorithms and applications," *Neural Networks*, vol. 13 (4-5), pp. 411-430, 2000.

48. A. T. Bell and T. J. Sejnowski, "An information maximization approach to blind separation and blind deconvolution," *Neural Computation*, vol. 7 (6), pp. 1004-1034, 1995.

49. J. F. Cardoso and A. Souloumia, "Jacobi angles for simultaneous diagnolization," *SIAM J. Mat. Anal. Appl.*, vol. 17 (1), pp. 145-151, 1996.

50. A. Le Couteur, M. Rutter, C. Lord, P. Rios, S. Robertson, and M. Holdgrafer, "Autism Diagnostic Interview: a standard investigator based instrument," *Journal of Autism Disorders*, vol. 19, pp. 363-387, 1989.

51. C. Lord, P. DiLavore and S. Risi, Autism Diagnostic obsertvation schedule, Los Angeles: Western Psychological services, 1999.

52. American Psychiatric Association, Diagnostic and Statistical Manual of mental disorder, DSM-IV 4th edition, Washington (DC): American Psychiatric Association, 1994.

53. R. W. Cox, "AFNI: Software for analysis and visualization of functional magnetic resonance neuroimages," *Computers and Biomedical Research*, vol. 29 (3), pp. 162-173, 1996.

54. R. W. Cox, A. Jesmanowicz., "Real-time 3D image registration for functional MRI," *Magnetic Resonance in Medicine*, vol. 42 (6), pp. 1014-1018, 1999.